NREL/TP-451-7163 • UC Category: 1262 • DE94011887

Microscopic Origins of Metastable Effects in a-Si:H and Deep Defect Characterization in a-Si,Ge:H Alloys

Final Subcontract Report
1 February 1991 – 31 January 1994

J. D. Cohen
University of Oregon
Eugene, Oregon

NREL technical monitor: B. von Roedern

National Renewable Energy Laboratory
1617 Cole Boulevard
Golden, Colorado 80401-3393
A national laboratory of the U.S. Department of Energy
Managed by Midwest Research Institute
for the U.S. Department of Energy
under contract No. DE-AC36-83CH10093

Prepared under Subcontract No. XG-1-10063-1

September 1994

rp MASTER

Available to DOE and DOE contractors from:
Office of Scientific and Technical Information (OSTI)
P.O. Box 62
Oak Ridge, TN 37831
Prices available by calling (615) 576-8401

Available to the public from:
National Technical Information Service (NTIS)
U.S. Department of Commerce
5285 Port Royal Road
Springfield, VA 22161
(703) 487-4650

Printed on paper containing at least 50% wastepaper and 10% postconsumer waste

DISCLAIMER

PREFACE

This Final Technical Report covers the work performed at the University of Oregon for the period 1 February 1991 to 31 January 1994 under NREL Subcontract Number XG-1-10063-1. The following personnel participated in this research program:

NAME	TITLE	WORK PERFORMED
J. David Cohen	Principal Investigator	Program Manager
John Hautala	Research Associate	ESR Measurements, a-Si:H Stability Studies
Thomas Unold	Research Assistant	Capacitance Characterization of a-Si,Ge:H Alloys (photo-CVD samples).
Fan Zhong	Research Assistant	Modulated Photocurrent and Capacitance Characterization studies of a-Si,Ge:H glow discharge samples.

TABLE OF CONTENTS

LIST OF ILLUSTRATIONS

LIST OF TABLES

EXECUTIVE SUMMARY

Our research supported by NREL Subcontract XG-1-10063-1 over the past three years has involved, first of all, a fairly complete characterization of a two series of a-$Si_{1-x}Ge_x$:H samples: a series of 9 films grown at the University of Delaware by the photo-CVD method (for $0.29 \leq x \leq 0.62$) and series of 6 films grown at U.S.S.C. by the glow discharge method (for $0.20 \leq x \leq 0.50$). Both these series of samples seem to represent what is close to the "state-of-the-art" in current a-Si,Ge:H alloys. Our detailed comparison of the properties of the glow discharge material with the photo-CVD samples show remarkable similarities rather than significant differences. In particular, our measurements of theses samples: (1) Allowed us to assign defect energy levels from a detailed analysis of our transient sub-band-gap photocapacitance and photocurrent spectra. We found clear evidence for two distinct defect sub-bands, one at roughly midgap and the other in the upper half of the gap, above E_F. The shallow level was also found to exhibit a suppression of its thermal release of trapped electrons suggesting a large degree of defect relaxation. We also determined the energy dependence of these defect bands within the gap as the Ge alloy fraction, x, was varied. (2) We found the density of deep defects to increase exponentially with the germanium content. This detailed dependence can be accounted for using a spontaneous bond-breaking model using parameters that can be determined independently from the width of the Urbach tail and the positions and widths of the defect bands. *This result implies that the alloy samples we have studied may already be quite close to a definite lower limit to the defect densities that can be achieved in this material.* (3) We found that the trapping lifetimes related $\mu\tau$ products for holes decrease in direct proportion to the density of midgap defects in these samples, at least up to Ge fractions of 50at.%. (4) We have also made significant progress toward identifying both the optical and thermal defect transitions in the a-Si,Ge:H alloys.

In addition to our studies of the low gap materials, we also studied the effects of carbon impurities at the 1at.% level on the light-induced degradation of a-Si:H. Our results show significant effects at this level, particularly in that the carbon contaminated material does not seem to exhibit saturation in degradation compared to the most intrinsic sample. We also found that both the stable and light-induced defect levels increased with carbon at these contamination levels.

1.0 INTRODUCTION

The work carried out over the past 3 years under NREL Subcontract XG-1-10063-1 has concentrated upon the evaluation of the electronic properties of the low mobility gap a-Si,Ge:H alloys. In addition, we have also carried out one series of studies to assess the effects of carbon impurities on the stability of a-Si:H film.

Our experimental results are based on a variety of techniques sensitive to the properties of defect states in semiconductors: admittance spectroscopy, drive-level capacitance profiling, the modulated photocurrent method, transient photo-capacitance (and photocurrent) spectroscopy, and electron spin resonance. We were able to obtain two representative series of a-Si,Ge:H alloy samples: one series grown by the photo-CVD method by researchers at the Institute for Energy Conversion, and the other grown by the glow discharge method in collaboration with researchers at U.S.S.C. These samples cover a range of optical gaps between 1.3 to 1.6 eV. The a-Si:H samples with varying levels of carbon impurities were grown in-house.

Our characterization methods were used to determine electronic quantities important to the device performance of the low gap alloys: deep defect energies and densities, Urbach bandtail energies, and $\mu\tau$ products for holes. When correlated against the atomic compositions of our samples, the trends in the measured electronic properties with Ge fraction are quite clear and are predominantly independent of the growth method. Furthermore, we have discovered a direct relationship between the positions of the defect levels and the quantitative values of the defect densities. This suggests a definite limit to the quality of the low gap alloys that can be achieved. In a few samples we have also investigated the changes in electronic properties caused by light induced degradation, but results for this part of the study are still preliminary.

In our studies of the role of carbon impurities on the light induced degradation of a-Si:H samples, we have established definite deleterious effects at the 1at.% level. We found that such levels of carbon typically increased the light-induced metastable defect density by a factor of 2 and, perhaps more significantly, impeded the saturation of the degradation effects quite seriously.

In the Sections that follow, we first describe the samples studied and review the experimental techniques employed. In Section 4 and 5 we present our detailed results on the electronic properties of the a-Si,Ge:H alloy samples. In Section 6 we present our results on light induced effects in the carbon contaminated a-Si:H samples and some preliminary results of degradation studies in the a-Si,Ge:H alloys. Finally, in Section 7 we summarize our findings and draw some general detailed conclusions.

2.0 SAMPLES

2.1 SAMPLE GROWTH

The samples utilized in this study were produced by a variety of methods. A majority of the a-Si,Ge:H samples studied were grown using the photo-CVD method by our collaborators at the Institute for Energy Conversion (C. Fortmann and Wayne Buchanen).[1] In this method SiH_4/GeH_4 gas mixtures are subjected to UV radiation which excites a dilute component of Hg atoms in the gas mixture. These Hg atoms collide with the reactants to produce SiH_n and GeH_n radicals which then adhere to the substrate to produce the a-$Si_{1-x}Ge_x$:H film. A series of 9 samples (including endpoint samples of pure a-Si:H and a-Ge:H) were grown on p^+ crystalline Si substrates using SiH_4/GeH_4 gas ratios varying between 3% to 15% (giving samples with Ge content ranging between 30at.% to 62at.%). The substrate temperature for all samples was 230°C and the reactor pressure was 5 torr. Total gas flows were typically 70sccm.

In addition, six glow discharge a-Si,Ge:H samples were obtained from S. Guha and J. Yang at U.S.S.C. These were also deposited on p^+ crystalline Si substrates using mixtures of Si_2H_6 and GeH_4 gases diluted in H_2. The GeH_4 flow rate was again varied to obtain the different Ge fractions. The substrate temperature was 300°C. More details on the deposition parameters are given elsewhere [2]. The 5 films we have been able to fully characterize had Ge compositions at 20at.%, 30at.%, 32.5at.%, 42at.%, and 50at.%.

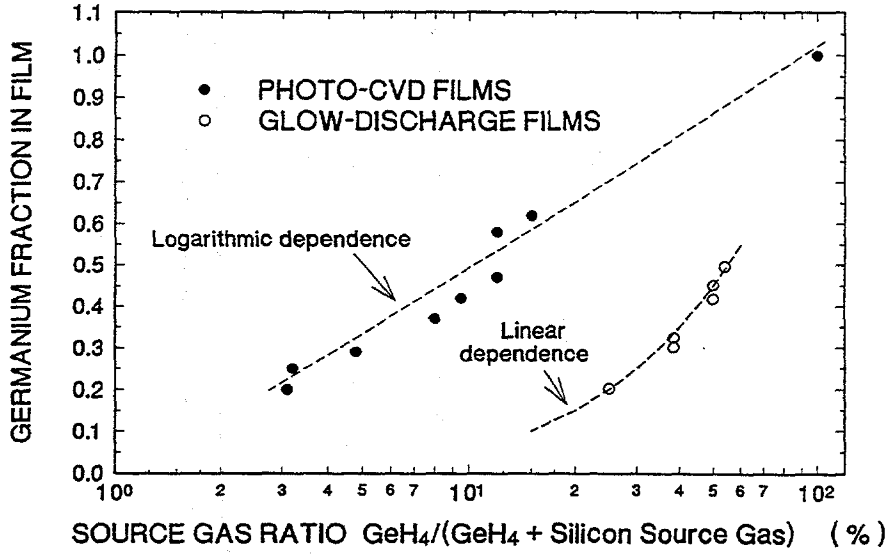

FIG. 1. Germanium fraction in our alloy films as a function of the $GeH_4/(SiH_4+GeH_4)$ source gas ratios for the photo-CVD films, and the $GeH_4/(Si_2H_6+GeH_4)$ ratios for the glow discharge films. The Ge fractions were determined by electron microprobe measurements carried out at NREL. For both sets of films the source gases were further diluted in H_2.

The germanium fraction, x, for each of the alloy samples was determined using electron microprobe measurements with a 5 keV beam energy. These measurements were carried out courtesy of Harv Mahan and Alice Mason at NREL. In Fig. 1 we plot the actual Ge fraction in each film *vs.* the GeH_4 ratios in the source gas. It is interesting that this graph indicates a roughly logarithmic dependence of Ge content on the gas ratio for the photo-CVD films, but nearly a linear dependence for the glow discharge produced alloys.

Finally, for the studies of light-induced degradation in a-Si:H with varying carbon content, we produced 3 samples in our in-house glow discharge reactor. These samples were grown using SiH_4 gas diluted 1:1 in Argon for a substrate temperature of 200°C. The carbon impurities were introduced using CH_4 gas and the actual concentrations in the films were determined by SIMS. The three samples studies had carbon concentrations of 0.006at.%, 1.0at.% and 2.6at.%.

2.2 SAMPLE PREPARATION

We deposited a 0.5mm diameter (area = 2×10^{-3} cm^2) semitransparent Pd contact on the top surface of each sample. After annealing the sample with the contact for about 30min at 200°C, a $PdSi_2$ Schottky barrier is formed. Our test devices thus consist of a p^+ buried junction at the c-Si substrate in series with the Pd Schottky at the film surface. Each sample was mounted on a transistor header using In-Ga eutectic on the back of the substrate to make an ohmic contact to the c-Si.

For the studies of light-induced degradation of the a-Si:H films, we exposed these samples to 647nm light from a Kr ion laser at 4.5 W/cm^2 for times varying between 1 and 10^5 seconds (20 hours). The stated intensity is corrected for the semi-transparent Pd contacts. To avoid heating the sample at this intensity level (which would anneal away some of the light induced effects), we immersed these samples in methanol during exposure. This ensured that the temperature of the sample surface was always maintained below 65°C.

Some preliminary studies were also made of the effects of light-induced degradation on the a-Si,Ge:H alloys. Here we employed tungsten-halogen light sources at intensities between 100 to 400 mW/cm^2 and exposure times between 50h and 800h.

3.0 EXPERIMENTAL METHODS

The measurements employed in our studies rely on a set of experimental techniques which have all been described previously in some detail. For the purpose of this report we will describe each method briefly and review what kind of information is obtained from each type of measurement.

3.1 ADMITTANCE SPECTROSCOPY

Our Schottky diode samples contain a depletion region which is characterized as a function of temperature and frequency before we undertake the more sophisticated capacitance based measurements described in Sections 3.2 and 3.4 below. Such measurements provide us with an estimate of our film thickness (the temperature independent region at low T is simply related to the geometric thickness, d, by the formula $C = \varepsilon A/d$), and an Arrhenius plot of the frequency of the lowest temperature capacitance step (or conductance peak) *vs.* 1/T provides us with the activation energy of the ac conductivity, E_σ,[3] which we identify with the Fermi energy position: $E_\sigma \approx E_C - E_F$. These admittance measurements also give us an indication of the quality of our Schottky barriers which allow us to pre-screen our samples for further study.

3.2 DRIVE-LEVEL CAPACITANCE PROFILING

The drive-level capacitance profiling method has been described in detail in many publications [4,5]. It is similar to other kinds of capacitance profiling in that it provides us with a density vs. distance profile; however, this particular method was developed specifically to address the difficulties encountered in interpreting capacitance measurements in amorphous semiconductors. In this method we monitor the junction capacitance both as a function of DC bias, V_B, and as a function of the amplitude of the alternating exciting voltage, δV. One finds that to lowest order this dependence obeys an equation of the form:

$$C(V_B, \delta V) \quad = \quad C_o(V_B) + C_1(V_B)\,\delta V + \ldots$$

and that the ratio

$$N_{DL} \quad \equiv \quad \frac{C_o{}^3}{2q_e\,\varepsilon A^2\,C_1} \qquad (1)$$

is directly related to an integral over the density of mobility gap defect states:

$$N_{DL} \equiv \int_{E_C-E_e}^{E_C-E_F^{\circ}} g(E)\,dE \quad . \qquad (2)$$

Here E_F^o is the bulk Fermi level position in the sample and E_e depends on the frequency and temperature of measurement:

$$E_e(\omega,T) = k_B T \log(\nu/\omega) \qquad (3)$$

Thus, by altering the measurement temperature (or frequency) we obtain information about the energy distribution of the defects and, by altering the applied DC bias, we can vary the spatial region at which we detect the defects in the sample. That is, we can spatially profile the defects as a function of the position from the barrier interface.

Typically we employ 100Hz profiles for a series of temperatures between 320K to 380K. In Fig. 2 we show an example of such a series of measurements for a USSC a-Si,Ge:H sample where we have extended the upper range of measurement to 400K to show the clear upper limit for N_{DL} which we associate with the total defect density (in a-Si:H we believe this upper limit is reached after uncovering only a fraction of the defect band and thus usually multiply this value by a factor of 2). This provides us with a quantitative measurement of the deep defect levels in these samples. In addition, we are able to assess the spatial uniformity of the electronic properties in these samples.

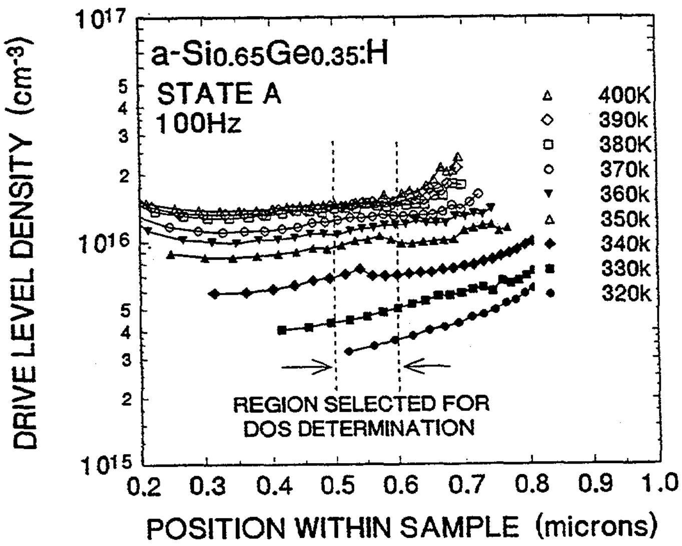

FIG. 2. Drive-level capacitance profiles for an a-Si,Ge:H sample produced by the glow discharge method at U.S.S.C. The 100Hz measurements were made at the temperatures indicated.

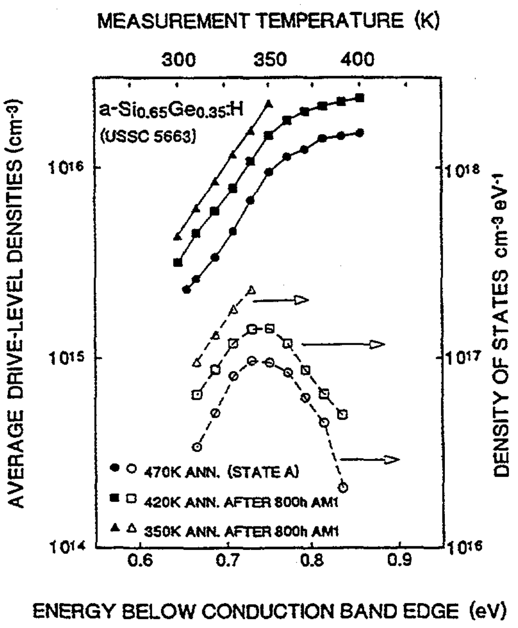

FIG. 3. Drive-level densities vs. energy depth obtained for data of Fig. 2 plus 2 metastable states. The energy derivates of these curves give the densities of states which are shown in the lower curves.

We can reconstruct the energy distribution of gap states as well. For a particular spatial region (near 0.55μm in Fig. 2) we plot in Fig. 3 the value of N_{DL} vs. the energy E_e given by Eq. (3). Then, by differentiating this curve with respect to E_e [see Eq. (2)] the density of states is obtained directly. In the case of this a-Si,Ge:H sample we obtain a clear picture of a defect band centered at $E_C - E_e = 0.75$ eV. The variation of the magnitude of this defect with metastable treatment is also shown and indicates a factor of 3 increase in this defect band after 800h of AM1 light exposure.

3.3 THE MODULATED PHOTOCURRENT METHOD

The modulated photocurrent (MPC) method was developed as a means to deduce the thermal energy distribution of mobility gap states that are normally unoccupied in equilibrium.[6,7] Thus, it is a quite complementary method to capacitance profiling which gives the thermal energy distribution of states normally occupied by electrons in thermal equilibrium in the bulk. In this method a sample is illuminated by above band-gap light ($h\nu \geq 1.8$eV) which varies sinusoidally with time. The magnitude and phase shift of the resulting photocurrent reveals the thermal emission rates of carriers trapped in normally unoccupied defect states. To carry out such measurements over an extended frequency range, we utilize fast light emitting diodes (with peak fluxes at wavelengths 560nm and 650nm) that are easily modulated from 5Hz to 100kHz. We employ intensities as small as possible to minimize any perturbations in the gap state occupation from those present in steady-state. The resulting photocurrent phase lag, ϕ, and modulus per area, $|I_{ac}|/A$ give the density of electron trapping states according to the relation [8]:

$$g(E_\omega) = \frac{2}{\sigma \langle v \rangle \pi k_B T} \left[\frac{q\, G_1 A\, m_e F}{|I_{ac}(\omega)|} \sin\phi - \omega \right] \qquad (4)$$

Here σ is the electron capture cross-section, $\langle v \rangle$ is the electron thermal velocity, q is electronic charge, G_1 is the sinusoidal component of the generation rate, is the free electron mobility, and F is the electric field. For a given temperature T, the energy depth E_ω is determined by the thermal emission rate of the electrons trapped in defect states; specifically: $E_\omega = k_B T \log(\nu/\omega)$, where ν is the thermal emission prefactor and ω is the angular frequency of the modulated light source. Thus, the density of states is determined using an energy scale that is identical to that corresponding to the drive-level capacitance profiling measurements described above.

In many cases our data is of sufficient quality that we may use an alternative derivative analysis of the modulated photocurrent signal. Such an analysis of the MPC spectra was recently proposed by Hattori et.al. [9] and it improves the energy resolution of the derived distributions significantly, from roughly k_BT to $k_BT/2$.

This method was implemented for the studies under our NREL Subcontract only fairly recently. Thus, these kinds spectra have only been obtained for a few samples. Also, unlike capacitance profiling, this method cannot provide absolute comparisons of defect densities and is thus less useful for routine characterization of our samples. However, this type of additional knowledge is quite crucial for our efforts to understand the defect structure of the a-Si,Ge:H alloys in detail (see Section 5.4 below).

3.4 TRANSIENT PHOTOCAPACITANCE AND PHOTOCURRENT

The general method of junction transient measurements on amorphous semiconductors has been discussed in detail in several earlier publications.[3,10,,11] The basic physics of all such measurements is as shown in Fig. 4. We illustrate the situation for a semiconductor with one discrete deep gap states within the space charge region of a Schottky barrier which is subjected to a voltage "filling pulse". This pulse causes a non-equilibrium (filled) occupation of gap state to be established. As time progresses, the initial steady-state population is recovered through the excitation of trapped electrons to the conduction band where they can then move out of the depletion region under the influence of the electric field. In the dark this process proceeds entirely by the thermal excitation of trapped carriers. However, this process can be enhanced through optical excitation which is the basis of the photocapacitance and junction photocurrent techniques.

The re-equilibration can be observed by the redistribution of trapped carriers, either as a change in the *junction capacitance* (which occurs because the depletion region will contract as negative charge is lost and the positive charge density increases) or by monitoring the *current* which results from the motion of this charge. However, the observation of capacitance transients has one significant difference compared to current transient measurements: The dominant type of emitted carrier (electron or hole) can be identified by the *sign* of the observed change in capacitance. Thus the direct comparison of capacitance and current transient measurements allows one to explicitly separate the electron and hole emission and/or transport processes.

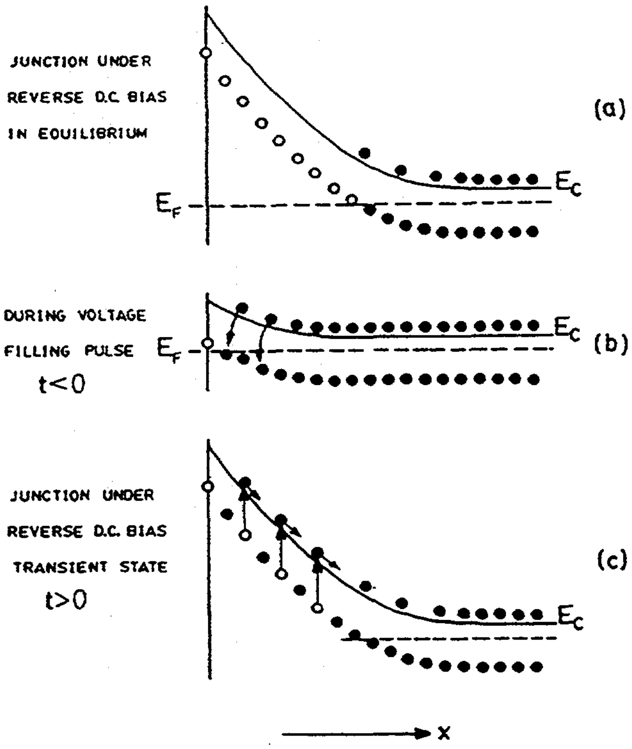

FIG. 4. Schematic diagram indicating the basic sequence of events in semiconducting junction transient measurements: (a) Junction under reverse bias in quasi-equilibrium showing the electronic occupation of gap states (solid circles) plus empty gap states above E_F in deep depletion (open circles). (b) During voltage "filling pulse" gap states capture electrons from the conduction band. (c) Reverse bias is restored and occupied gap states above E_F are slowly released to the conduction band due to thermal or optical excitation processes.

In our photocapacitance (or photocurrent) measurements we fix the temperature and record transients alternately in the dark and in the presence of sub-band-gap light. The experimental details to accomplish this have been discussed previously.[12,13,14] We then define the photocapacitance (or photocurrent) signal, $P(E_{opt})$, to be the photon flux (Φ) normalized difference in the integrated transient signals recorded with and without the presence of the sub-band-gap light of optical energy E_{opt}. The photocapacitance *spectrum* is obtained by plotting P *vs.* E_{opt} at constant T. We take special care to always operate in the low light intensity limit (where P is intensity independent). Thus the photocapacitance spectrum reveals the distribution of allowable transitions for an electronic population of gap states not appreciably disturbed by the optical excitation, but rather determined by the application of the voltage pulse followed by whatever thermal evolution takes place within the time before the transient is recorded.

Several examples of photocapacitance spectra are given in the following sections and have the general appearance of spectra obtained by the perhaps more familiar steady-state sub-band-gap optical techniques, such as photo-thermal deflection spectroscopy (PDS) [15] or the constant photocurrent method (CPM). [16] Indeed, one encounters a rather similar expression in the interpretation of our transient photospectra in terms of a convolution between localized gap states and extended states connected by an optical matrix element for the transitions. Specifically, for transitions from gap state electrons to the conduction band one expects a contribution to P given by [8,9]:

$$P_n{}^c(E_{opt},T) = K_n(T) \int_{E_c-E_{opt}}^{E_c-E_e} |<i|ex|f>|^2 \, g(E) g_c(E+E_{opt}) dE \qquad (5)$$

where $|<i|ex|f>|^2$ represents the optical matrix element, and $K_n(T)$ is a constant that depends on the temperature as well as the overall depletion width and the time window parameter τ (and also the frequency for the case of capacitance measurements). It will also depend on the ability of the carriers, once optically excited into the conduction band, to leave the depletion region. Thus K will depend on the electric field distribution within the depletion region and the electron mobility. However, all of these factors will be roughly constant (independent of optical energy) for a given temperature and applied bias. One should also note that the upper limit of the integral is determined by the thermal escape depth, E_e, of gap state electrons to the conduction band at the measurement temperature and time window, τ, as given by Eq. (3) with $1/\tau$ substituted for ω. That is, the optical transitions from these shallower electronic levels will be missing from the photocapacitance spectrum because they will have escaped thermally before the photocapacitance signal is recorded.

We should stress that the expression given in Eq. (5) represents only one contribution to the photocapacitance or photocurrent signals. A similar expression [giving a quantity we might label $P_p{}^v(E_{opt})$] must be included to take into account transitions from the valence band into empty gap states. The leading constant will then be replaced by $K_p(T)$ which contains information about how easily the optically excited holes will leave the depletion region.

There are actually two other sub-band-gap optical processes that must be considered as well. First of all, an electron from the valence band can be excited into an empty gap state that is close enough to E_c that it will subsequently thermalize into the conduction band. This will occur on the timescale of our measurement if it lies within an energy E_e of conduction band mobility edge, and can be represented by the integral

$$P_n{}^v(E_{opt},T) = K_n(T) \int_{E_c-E_e}^{E_c} |<i|ex|f>|^2 \, g(E) g_V(E-E_{opt}) dE \qquad (6)$$

With such a process there is also a hole left in the valence band. And, there will be an analogous integral expression for $P_p{}^c$ resulting from optical transitions from deep in the mobility gap to the conduction band such that the hole that is left in the gap will thermalize the valence band on the measurement timescale.

A schematic diagram indicating these four types of processes in given in Fig. 5. Without additional information it is obvious that a single type of sub-band-gap spectrum will not allow one to distinguish the above possible contributions responsible for the observed signals. For example, PDS measurements are totally insensitive to the subsequent motion of carriers and therefore have absolutely no way to distinguish between such different types of transitions. Some proponents of the CPM method argue that at low temperatures one can generally neglect the contribution of minority carrier motion to the current signal. However, one still has no way to separate the contributions to the electron current from the types of processes labeled (3) and (4) in Fig. 5. Indeed, the contribution of processes of type (3) has generally been completely neglected in the analysis of CPM spectra that have appeared in the literature.

Our studies, which compare the photocapacitance and photocurrent spectra resulting from the same set of electronic transitions, provide one of the few methods to identify the different types of transitions in Fig. 5 since these contribute differently for a photocapacitance as opposed to a photocurrent spectrum. The procedure followed to separate these is illustrated in detail in Section 5.1 below.

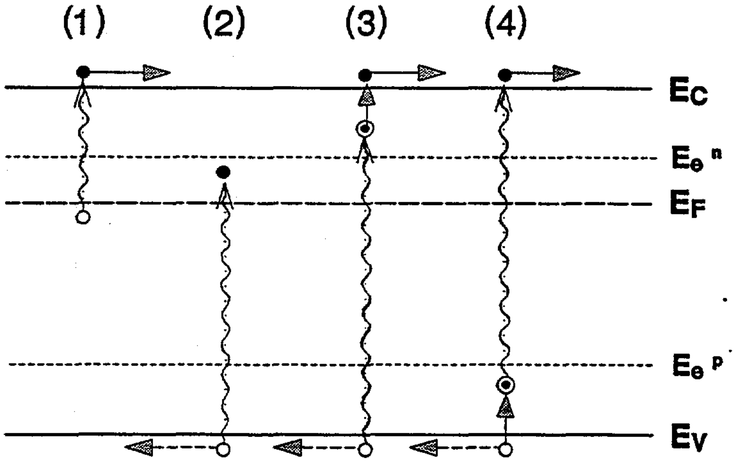

FIG. 5. Schematic diagram of the types of optically initiated deep defect transitions. As discussed in the text, these contribute differently to the photocapacitance and the transient photocurrent signals. Here optical transitions are indicated by wavy lines and thermal transitions are indicated by solid vertical lines. Horizontal arrows indicate electron and hole transport out of the depletion region. The dashed horizontal lines for the hole motion illustrate the fact that holes are more likely to be re-trapped before escaping the depletion region.

3.5 ELECTRON SPIN RESONANCE

Electron spin resonance (ESR) spectroscopy is generally used to determine the density of singly occupied deep defects. It provides an absolute density measurement, although it is insensitive to any population of charged defects. In the studies reported here this method is usually employed only in a secondary mode to corroborate the defect densities determined by our drive-level profiling method. In this regard we have been able to establish quite good agreement, to within a factor of 2, between the two techniques. To illustrate this, in Fig. 6 we exhibit a direct comparison of the absolute defect densities determined by these two kinds of measurements for an intrinsic a-Si:H glow discharge sample in which we vary the metastable defect density through an extended series of light soaking exposures and, following this, by a series of partial anneals back to state A. [17] The agreement between the absolute defect densities found by the 2 methods is extremely good. Such comparisons have allowed us to utilize with considerable confidence our drive-level technique as the primary tool for estimates of deep defect densities.

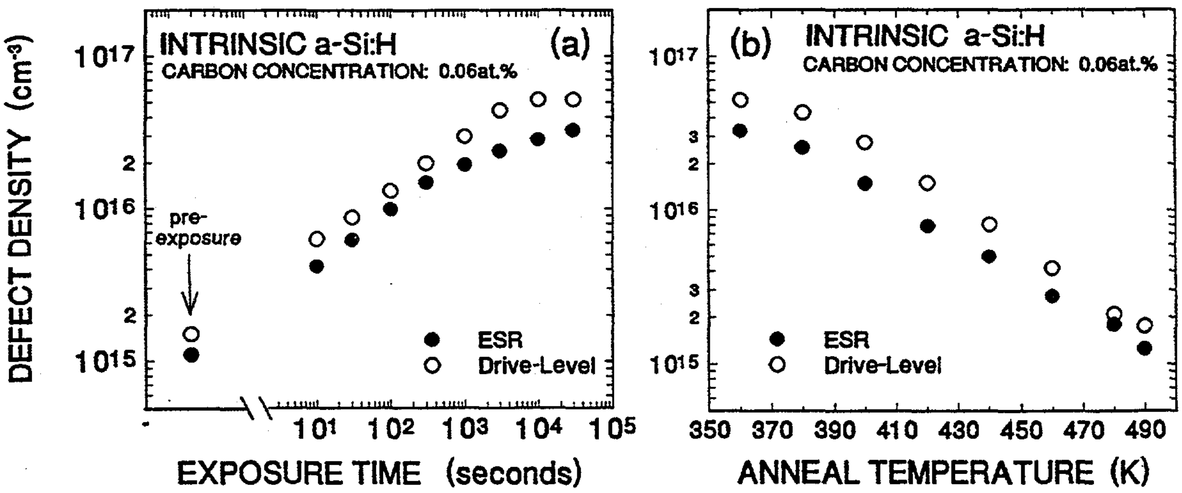

FIG. 6. Comparison of the density of defects as determined by drive-level capacitance profiling and ESR for an intrinsic a-Si:H sample. The defect density in this sample has been modified substantially through a sequence of light soaking steps and, following this, a series of partial anneals. The agreement between the absolute defect densities obtained by the two methods is seen to lie within a factor of two at each step within these series of metastable states.

4.0. BASIC ELECTRONIC PROPERTIES OF THE a-Si,Ge:H ALLOYS

4.1 OPTICAL GAPS AND URBACH SLOPES

As discussed in Section 3.4, our transient photocurrent and photocapacitance methods provide a sensitive way to record the sub-band-gap optical transition spectra arising from localized states in the mobility gap. In this Section we will present an overview of the results that are obtained from a single spectrum type, and we will often rely more on the photocurrent measurements since they exhibit superior signal to noise. However, the determination of bandtail energies and optical gaps is quite consistent from either the photocapacitance or photocurrent spectra. A more detailed analysis based on both types of spectra together is discussed in Section 5.

A series of transient photocurrent spectra for 6 of our photo-CVD grown a-Si,Ge:H samples is shown in Fig. 7(a) [18] and for 3 of our glow discharge samples in Fig. 7(b). [19] We can immediately utilize such spectra to determine the Urbach slopes and optical gaps. In Fig. 7 we observe that the photocurrent spectra begin to flatten for the highest optical energies. This occurs for two reasons: first, that we begin to see the rollover from the exponential tail regime into the quadratic density of states of the valence band; and, second, because the exciting light becomes more strongly absorbed at higher optical energies and thus cannot excite carriers equally over the entire depletion region. Because these two competing effects occur within a similar energy regime, it is difficult to assign optical gaps to these samples from our spectra. Fortunately, for a few alloy compositions we also had at our disposal companion films on transparent substrates so that we could accurately determine the optical gaps. We then compared these transmission spectra with the corresponding transient photo-spectra so that we could establish an algorithm for finding the optical gaps directly from these latter measurements.[20] The optical gaps determined in this fashion are plotted in Fig. 8.

In Fig. 8 we clearly observe a linear reduction of the optical gap with increasing Ge content, x, which can be expressed in the form

$$E_{gap} = 1.72\ \text{eV} - (0.625\ \text{eV})\ x \qquad (7)$$

This observed dependence agrees fairly closely with results obtained in studies of a-Si,Ge:H samples grown and characterized by other techniques [21,22].

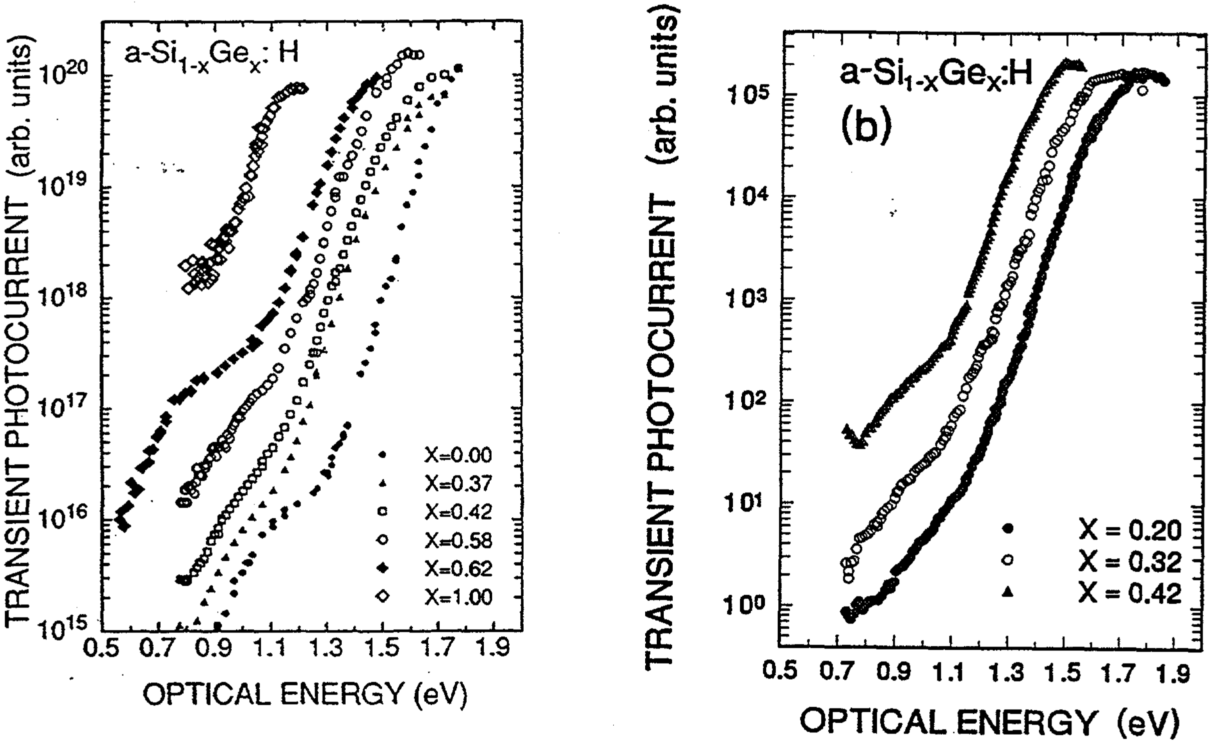

FIG. 7. (a) Transient photocurrent spectra for a series of six photo-CVD a-$Si_{1-x}Ge_x$:H films with different Ge fractions as indicated.
(b) Transient photocurrent spectra for a series of three glow discharge a-$Si_{1-x}Ge_x$:H films.

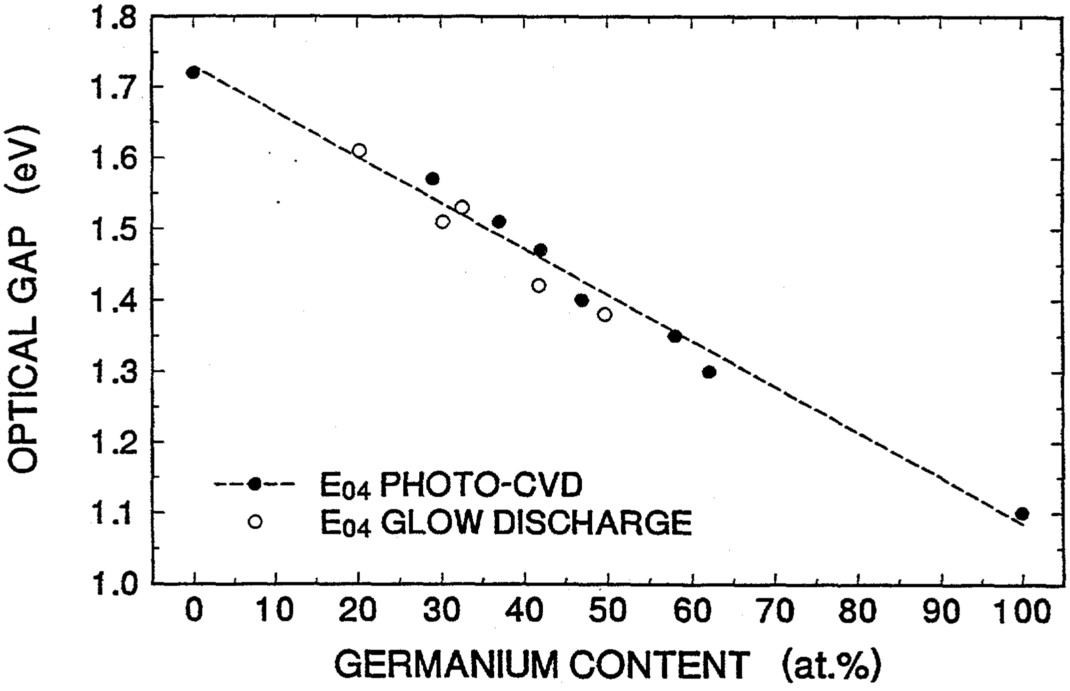

FIG. 8. Variation of the optical gaps, E_{04}, with the Ge fraction in our alloy films.

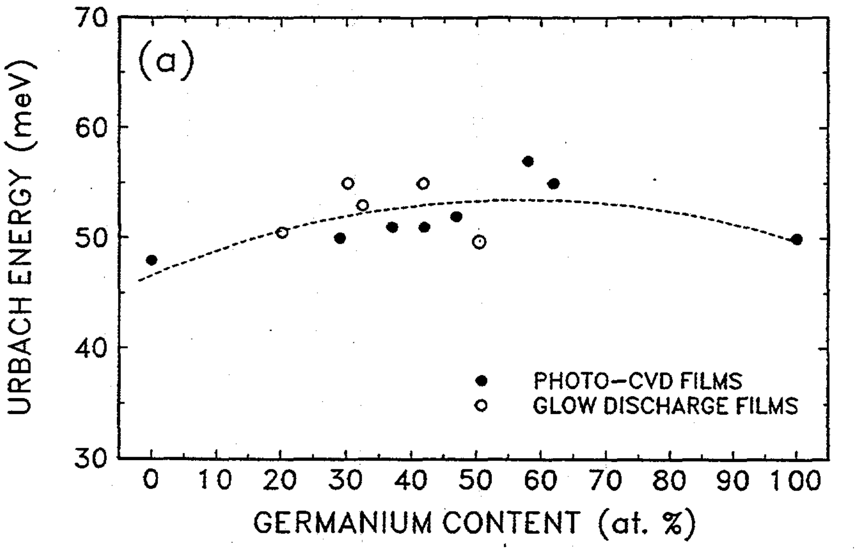

FIG. 9. (a). Variation of Urbach bandtail energies, E_U, with alloy composition. A relatively constant value of 53 ± 3 meV is indicated, roughly independent of Ge content. The dashed line is a guide to the eye which suggests that the endpoint films have somewhat narrower bandtails than the alloys in the middle of the composition range. (b) Comparison of E_U obtained for our photo-CVD samples with glow discharge samples of other groups as a function of the optical gap energy.

Exponential Urbach tail regions are easily identified for all the spectra of Fig. 7. The spectral dependence on optical energy, $h\nu$, in this region, $S(h\nu)$, obeys the functional form

$$S(h\nu) = S_o \exp[(E_{gap} - h\nu)/E_U] \qquad (8)$$

which defines the Urbach energy, E_U. The value of E_U obtained from our measurements is given in Fig. 9(a) as a function of Ge content and, in Fig. 9(b), as a function of optical gap. [20] In Fig. 9(b) we also show comparison data for samples grown by the glow discharge method as characterized by a couple other groups. We observe that the Urbach energies for the photo-CVD samples are roughly independent of alloy composition, lying in the range: $E_U = 53 \pm 3$ meV. The USSC glow discharge samples are quite comparable. Such values of E_U are comparable to the best a-Si,Ge:H alloy samples produced previously.

4.2 MIDGAP DEFECT DENSITIES

The photocurrent spectra in Fig. 7 all exhibit a shoulder to the left of the exponential bandtail regime. This is due to the presence of deep defect bands. The energy positions of these bands is obtained by an analysis of such spectra as described in Section 5. A more direct and quantitative estimate of the total deep defect densities in these samples is obtained by the drive-level profiling measurements, as discussed in Section 3.2.

In carrying out those measurements we can determine a limiting upper value to N_{DL} by repeating such profiles at increasing temperatures. For the a-Si,Ge:H alloys this value gives a quite good estimate of the total deep defect density provided we are able to obtain good profiles to high enough temperatures. However, in a-Si:H and some alloy samples we are not able to access the charge throughout the entire defect band. We can recognize such cases by the fact that N_{DL} does not reach a clearly defined asymptotic limit at high temperature. In such cases we can obtain a better estimate of the total defect density by doubling the value of N_{DL} at the temperature where N_{DL} vs. T has its maximum slope. As discussed in Section 3.4 this estimate has been found to be quite consistent with values of deep defect densities obtained from ESR measurements in a-Si:H samples.

Drive-level density estimates for 11 alloy samples (plus one of pure a-Ge:H) are plotted *vs.* Ge content in Fig. 10. [18,19] (Our defect density for the a-Ge:H sample

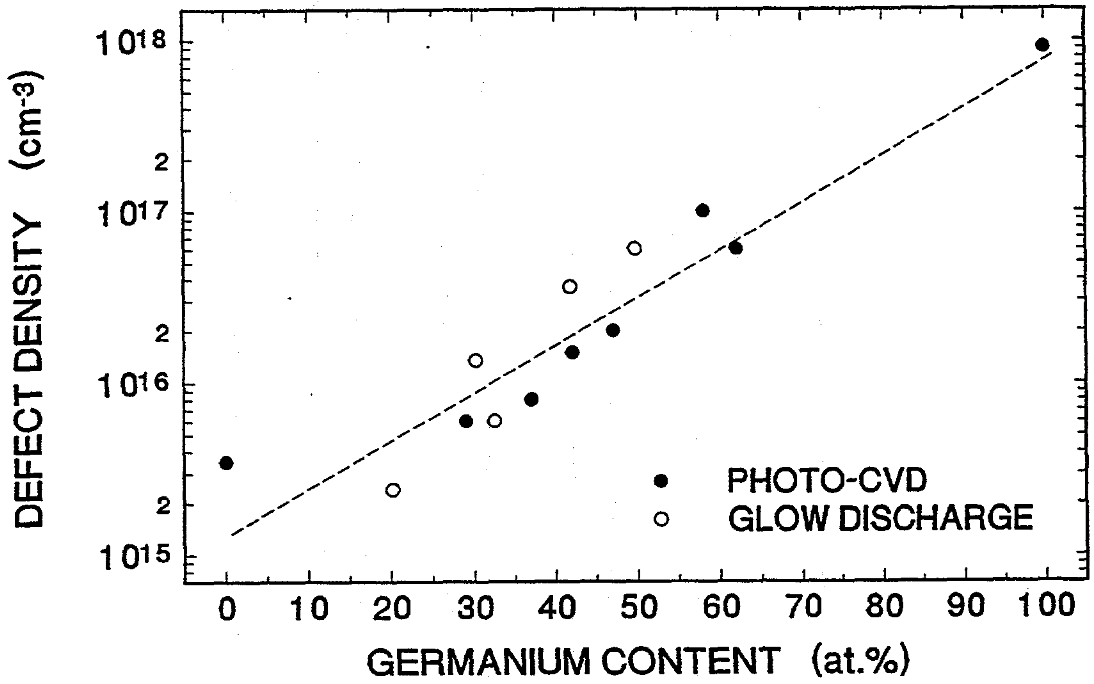

FIG. 10. Drive-level determined deep defect densities *vs.* the alloy composition for both the photo-CVD and glow discharge films. The dashed line indicates that the defect density increases exponentially with Ge content.

was actually estimated from an analysis of admittance *vs.* T measurements [23] since this sample was too thin for profiling measurements.) We see a quite consistent exponential dependence of the deep defect density vs. Ge content for both types the photo-CVD and glow discharge samples such that we get a factor of 10 increase as the Ge fraction is increased from 20at.% to 60at.%. Indeed, all but 3 of the alloy samples lie within a factor of 1.25 of this universal curve (see Fig. 10) and most of the remaining samples exhibited somewhat broader Urbach tail energies implying generally a larger degree of disorder than the vast majority of our alloy films.

The range of compositions corresponds to a variation in optical gap from 1.6 to 1.35eV. A very similar factor increase with decreasing optical gap has been reported by the Princeton group [21] for both D.C. and r.f. glow discharge alloy samples. They base their estimates on the integration of the defect band in CPM sub-band-gap absorption spectra. However, since they calibrate their absolute densities to values obtained using ESR, we can compare our results fairly directly. We thus conclude that the absolute defect densities for our samples are at least a factor of two smaller.

4.3 MINORITY CARRIER TRANSPORT

In this Section we shall examine the most readily accessible piece of new information that can be obtained once we begin comparing pairs of photocurrent and photocapacitance spectra taken under identical measurement conditions: namely, the escape probability of an optically induced free hole from the depletion region. This probability is directly related to the $\mu\tau$ product for holes in these alloy samples. Because of the long time scales of this measurement method the τ obtained is specifically a deep trapping time. Not surprisingly, for samples containing 50at.% Ge or less, we find that our measured $(\mu\tau)_h$ products are inversely proportional to the deep defect densities.

Figure 11 gives a comparison between the photocurrent and photocapacitance spectra for one a-Si,Ge:H sample at two different temperatures.[23] At low temperatures the curves are essentially identical. Because the junction current and capacitance transients have very different sensitivities to the spatial distributions of defects [24], this close match of the two spectra verifies that our samples are spatially quite uniform. At the higher temperature the spectra differ substantially and, as we discussed in Section 3.4, this difference can be entirely attributed to the motion of minority carriers.

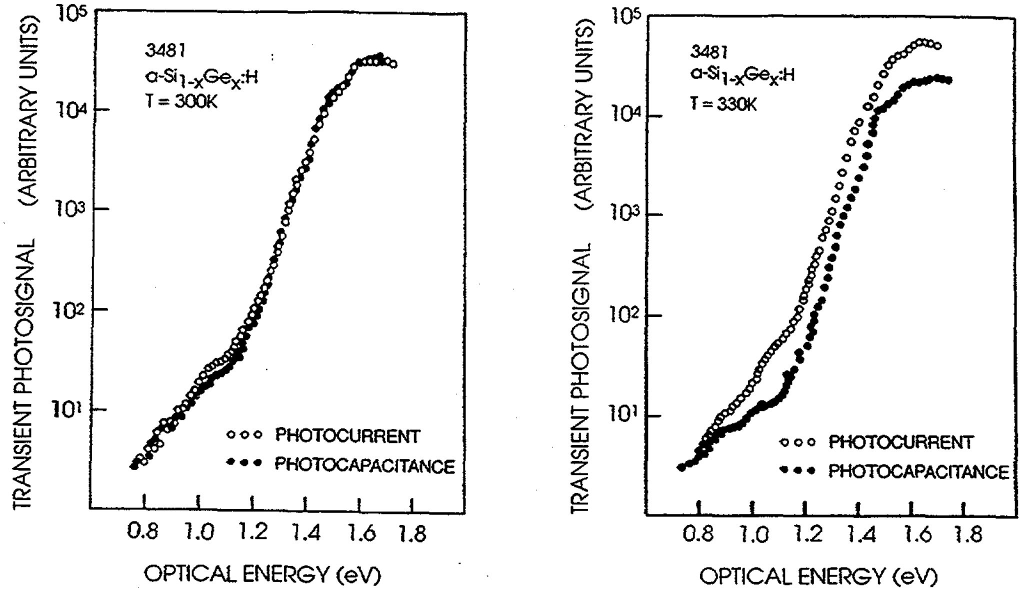

FIG. 11. Comparison of transient photocapacitance (solid circles) and junction photocurrent spectra (open circles) for an a-Si$_{1-x}$Ge$_x$:H sample (x = 0.47) at two temperatures as indicated. The capacitance measurement frequency was 1kHz and the transient measurement time window was 0.4 s. The two types of spectra have been overlapped in the lowest optical energy regime, and the differences observed between the higher temperature spectra indicate the existence of hole processes.

Specifically, the hole currents will *add* to any electron currents caused by the optically induced release of trapped carriers, but *subtract* from the resultant charge changes in the depletion region, as monitored by the photocapacitance technique. Such effects are small at lower temperatures since the hole motion is minimal (effective hole mobilities are small and so they are quickly retrapped). At higher temperatures, however, the net motion of the holes increases to cause significant differences between the spectra.

When such differences exist we choose to align the two types of spectra at the lowest optical energies. This makes sense referring back to Fig. 5 since, at the lowest optical energies, we expect only to be able to excite a single carrier type [transition (1) in Fig. 5]. Thus the two types of spectra can be calibrated by matching them to each other in this energy regime. Following this procedure in Fig. 11, we then observe that the ratio of the photocapacitance and photocurrent signals in the bandtail region (optical energies greater than about 1.2 eV) differ only by a constant factor. This happens because optical excitation near the optical gap leads to the generation of free electrons and holes in roughly equal numbers. [See transitions (3) and (4) in Fig. 5] If both types of carriers were to escape the depletion region with equal probability, the net charge change, and hence the transient photocapacitance signal, would be nearly zero. However, the transient photocurrent signal would be enhanced. In general, then, the degree of suppression of hole escape will increase the relative ratio, R, of the photocapacitance to the photocurrent signals, and this ratio can be used to determine the retrapping distance of the liberated hole, and hence $(\mu\tau)_h$.

As presented in detail elsewhere [14,20,25], we have derived an explicit expression for $(\mu\tau)_h$ in terms of R and the charge density, N_+, in deep depletion of our sample. This latter quantity is obtained experimentally by our drive-level profiling measurements in the limit of increasing temperature (as discussed in Section 4.2). We obtain [26]

$$(\mu\tau)_h \quad = \quad \frac{\varepsilon}{q_e N_+} \log\,[(R+1)/2R] \qquad (9)$$

We can illustrate the use of this formula for the data exhibited in Fig. 11. The ratio for optical energies above $h\nu = 1.3\text{eV}$ is roughly constant at $R = 0.27$, and our drive level measurements give $N_+ = 1.5 \times 10^{16}\ \text{cm}^{-3}$. Hence we obtain $(\mu\tau)_h = 5 \times 10^{-10}\ \text{cm}^2/\text{V}$. Note that the value we obtain depends on the measurement temperature [that is, compare Figs. 11(a) and 11(b)] but reaches a limiting value as temperature is increased. It is this limiting value that we report. Indeed, our $(\mu\tau)_h$ evaluation is quite consistent with trapping time derived $(\mu\tau)_h$ products determined by other methods [21].

In a like manner we have determined $(\mu\tau)_h$ for most of our other a-Si,Ge:H samples. The dependence of this quantity on Ge content, x, is displayed in Fig. 12(a). [8] We clearly observe a monotonic *decrease* in $(\mu\tau)_h$ as the Ge fraction is increased. Since the density of defects *increases* in this region, the observed decrease in $(\mu\tau)_h$ may simply reflect the increased likelihood of deep trapping due to the extra defects. Thus in Fig. 12(b) we plot the product $(\mu\tau)_h N_D$ *vs.* x. Here we observe a fairly constant dependence except at the very largest Ge fraction. The observed marked decrease in $(\mu\tau)_h N_D$ for $x > 0.5$ is perhaps due to a larger hole capture cross-section which could be due to an increased fraction of charged defects for the higher Ge containing alloys.

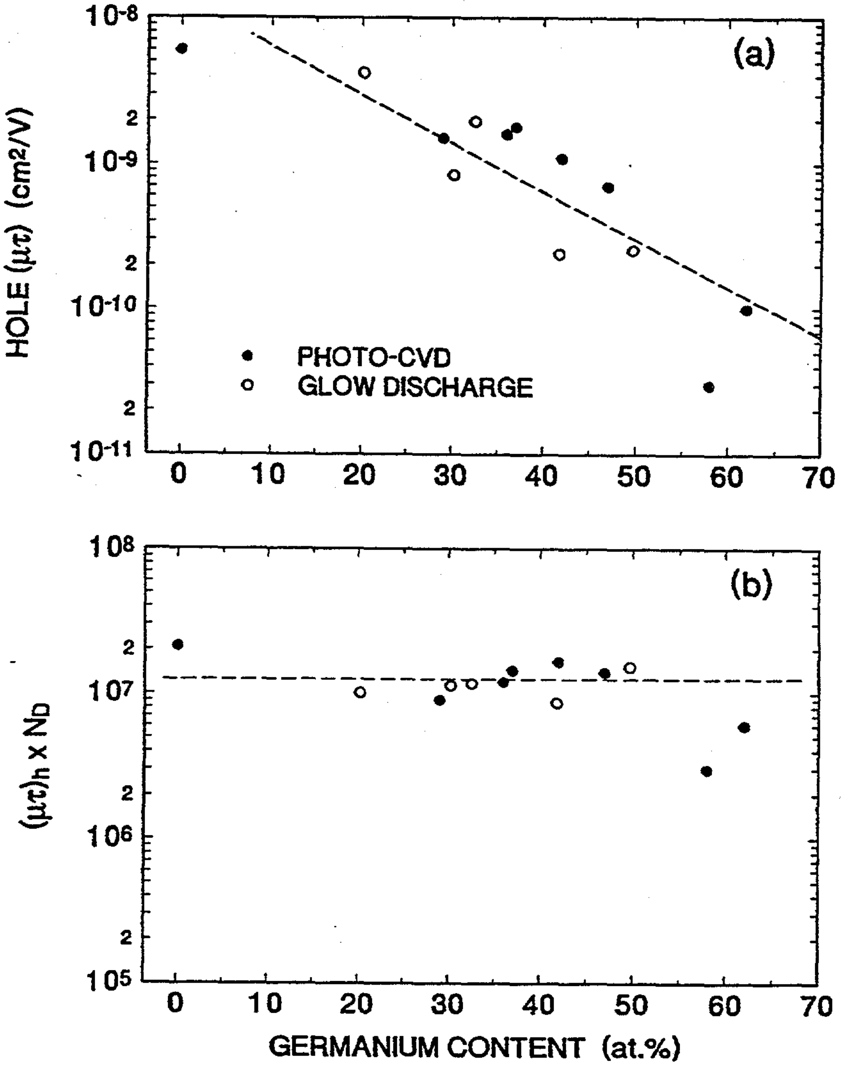

FIG. 12. (a) Dependence of the hole $\mu\tau$ products deduced from the analysis of the photocapacitance/photocurrent ratios on alloy composition. (b) The variation of $(\mu\tau)_h$ multiplied by the corresponding defect densities [that is, $(\mu\tau)_h N_D$] on the alloy composition, indicating a nearly constant dependence.

5.0 DEEP DEFECT ELECTRONIC TRANSITIONS IN THE a-Si,Ge:H ALLOYS

5.1 DEFECT RELATED OPTICAL TRANSITIONS

In this Section we discuss what can be learned about the deep defects through the detailed analysis of transient photocapacitance and photocurrent spectra taken together. In the previous section we learned that, for such pairs of spectra obtained at higher measurement temperatures, one could identify the electron from the hole processes initiated by optical transitions. Such differences arise because the motion of electrons and holes out of the depletion region both give the same sign current, and thus contribute additively to the photocurrent signal, but result in opposite changes to the total depletion charge, and thus contribute subtractively to the photocapacitance signal.

As discussed in our previous annual reports and elsewhere [12,18,25,27], we have able to successfully model both types of spectra together by incorporating the set of optical transitions shown schematically in Fig. 13. This analysis, described in more detail below, has yielded the following general conclusions for all the alloy samples studied: (1) There exists a well defined set of defect transitions for a band located near midgap [transition (a) in Fig. 13]. It is this defect band which we believe to be connected with the defect densities determined by our drive-level profiling measurements. (2) There exists a second well defined defect band above midgap and also above the Fermi energy. This defect band gives rise to transitions from the valence band [transition (b)] with an accompanying motion of the residual valence band hole. However, we have determined that the subsequent thermal emission of the electron that was excited into the empty defect state is greatly suppressed, even at elevated temperatures. (3) There exist a combination of valence band or valence bandtail to conduction band or conduction bandtail transitions [transitions (c) and (d)] which result in the Urbach exponential tail part of each spectrum. The magnitude of the photocapacitance spectrum is suppressed at higher temperature, however, due to resultant hole motion. Indeed, it was the ratio of the magnitudes of the photocapacitance and photocurrent signals in this energy regime (which is roughly constant) that allowed us to establish the deep trapping $\mu\tau$ products of these holes described in Section 4.3 above.

In Figure 14 we show an example of the quality of fits we are able to achieve for the pair of photocapacitance and photocurrent spectra for the photo-CVD grown a-$Si_{1-x}Ge_x$:H film with x=0.47. [18] This fit requires us to incorporate two bands of defect transitions: one broader band near midgap (near E_c - 0.76eV) *from which* we can excite electrons into the conduction band, and a narrower band *to which* we can excite electrons from the valence band. This second band of transitions has a much larger optical threshold (1.02eV); however, the strength of the two transitions are nearly the same. The second band results in photogenerated free holes which lead to the significant splitting of the two types of spectra near 1.1 eV.

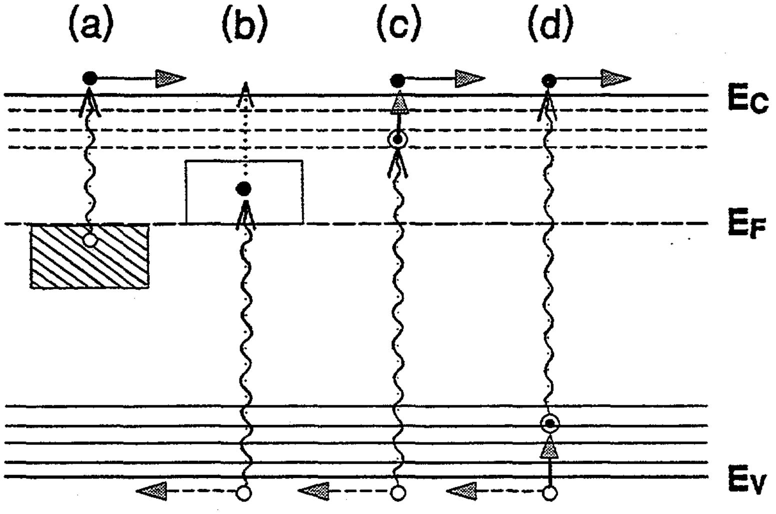

FIG. 13. Schematic of optical transitions (wavy lines) and thermal transitions (dashed lines) incorporated in the modeling of the a-Si,Ge:H photocapacitance and photocurrent spectra obtained experimentally. The dotted line for the thermal transition step in process (b) indicates that the electron emission for this process is suppressed.

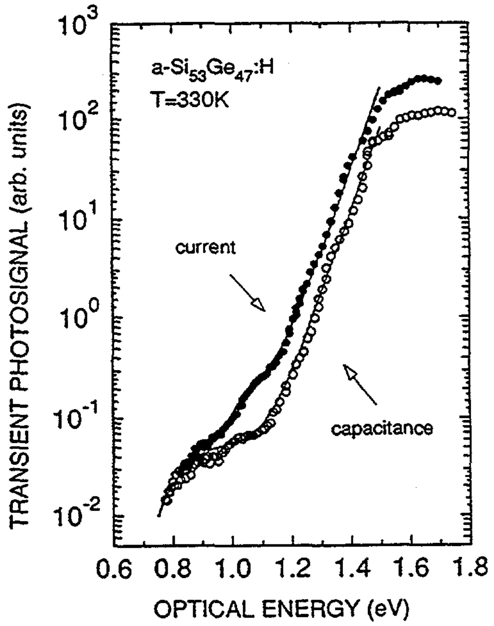

FIG. 14. Fits (solid lines) to the photocapacitance and transient photocurrent spectra for a photo-CVD grown sample containing 47at.% germanium. These fits were obtained employing the types of defect transitions shown in Fig. 13. In particular, a transition of type (a) was incorporated involving a defect band 0.75eV below Ec with a FWHM of about 0.3 eV, and a transition of type (b) lying 1.02eV above Ev with a FWHM of about 0.1eV.

These two defect transitions correspond closely to transitions (a) and (b) shown in our schematic diagram (Fig. 13). The somewhat surprising aspect of this analysis is that the electrons introduced into the gap from valence band for the second type of transition has a sufficiently large optical threshold that one would normally expect it to be re-emitted into the conduction band. However, the re-emitted fraction at 330K is only about 30%. This large thermal barrier suggests that electrons placed into this defect sub-band may undergo significant lattice relaxation. This conclusion is also consistent with recent findings by the Tauc group [28] based upon photo-induced absorption studies of a-Si,Ge:H alloys. This unusual aspect of defect dynamics may have significant deleterious consequences on electron transport in the alloys, as has been discussed by other researchers [29,30].

The existence of this second band of defect transitions is to be contrasted with all of our previous studies on amorphous silicon which indicate only a single band of deep defect related optical transitions. The second band of transitions is nonetheless clearly observed in all the a-Si,Ge:H films we have studied to date. It manifests itself most dramatically for one of the U.S.S.C. glow discharge samples shown in Fig. 15. Here its transition rate is strong enough that, at its optical threshold, the hole signal actually exceeds the electron signal thus causing the photocapacitance signal to *change sign*.. In spite of the complicated appearance of the spectra in Fig. 15(b), it is still fit quite well with two bands of optical transitions qualitatively identical to those of the other samples. The main difference is that the strength of the second transition for this sample is roughly 25 times as strong as the midgap band of transitions. Moreover, the dramatic variation of the appearance of these spectra with temperature is almost entirely due to the temperature dependence of the hole escape probability -- from about 0.82 at 350K to 0.29 at 320K. That is, the parameters describing the positions, widths, and strengths of the two defect bands are essentially temperature independent. [27]

The large asymmetry between the strengths of the two optical bands in this sample contrasts with most of the other samples studied. We believe that it comes about because this sample is actually very slightly p-type (that is, π-type). Although this sample was not doped [31], its π-type character is clearly manifested in the fact that, following light soaking, the activation energy of conduction is observed to *decrease*. (In almost all of our other samples tested in this fashion, this activation energy was found to increase or remain unchanged.) Recognizing the π-type character of this sample is very important in efforts to identify these optical transitions (see Section 5.4).

In Figure 16 we plot the positions of the two defect bands as a function of the Ge content in each sample. The optical gap energies are also plotted for comparison. We observe that the midgap defect band tracks more closely conduction band edge than the valence band edge so that its nearly midgap position in the lower Ge alloys tends to become slightly deeper than midgap as we move toward pure a-Ge:H.

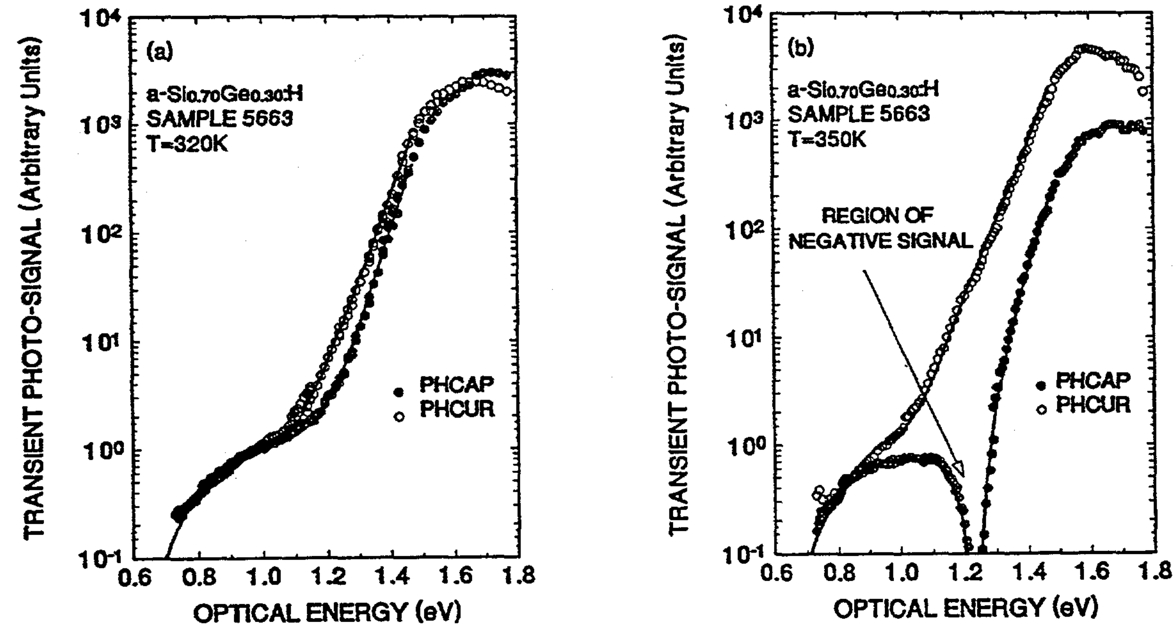

FIG. 15. Two pairs of transient photocapacitance and photocurrent spectra for a U.S.S.C. glow-discharge a-Si,Ge:H sample containing 30at.% Ge. The solid lines are the result of model fits to the types of transitions shown in Fig. 13. Because of the strength of the defect transition of type (b) for this sample, and the high $\mu\tau$ product for holes, the photocapacitance actually changes sign near an energy of 1.2eV. The shapes of these spectra are seen to vary dramatically with temperature; however, this comes about almost entirely from the variation of the free hole $\mu\tau$ with temperature, not on any significant changes in the defect transitions themselves.

FIG. 16. Energy positions (with respect to the valence band mobility edge) of the two defect bands inferred by the modeling of the photocapacitance and photocurrent spectra according to the transition processes shown in Fig. 13. The energy of the optical gap (E_{04}) for each of the films is also shown for reference.

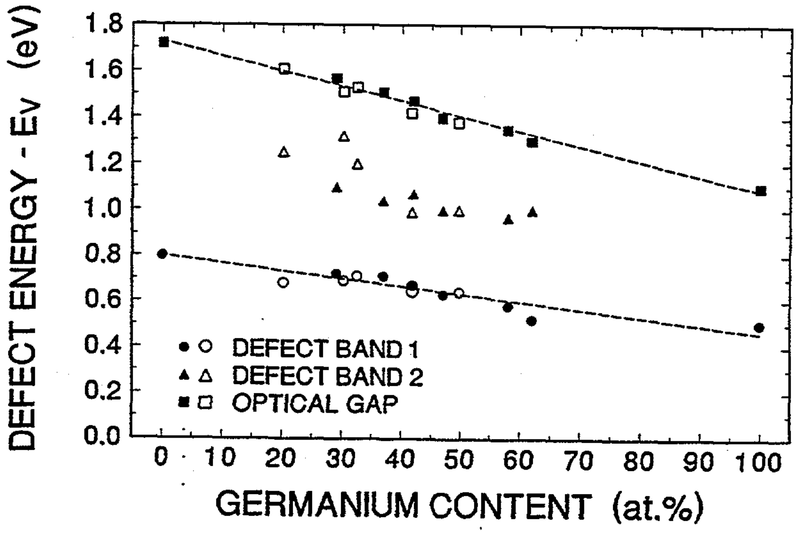

5.2 RELATION BETWEEN OPTICAL SPECTRA AND DEFECT DENSITIES

The total density of defects for our a-Si,Ge:H samples was deduced from drive-level capacitance measurements as discussed in Section 4.2. The defect density was found to increase exponentially with increasing germanium content, a functional behavior that is in agreement with a number of other studies. [21,32,33,34] However, the defect densities of our samples are lower than most of the values reported elsewhere. Furthermore, most of those studies reported an exponential growth of the defects accompanied by an increasing slope of the Urbach tail. This correlation is not present for our films.

The markedly higher defect densities for the samples with large germanium content have usually been attributed to a non-optimized growth condition leading to more defective samples.[35] Others have suggested that the exponential increase in defect density is consistent with weak bond breaking models that assume thermal equilibrium between band tail states and deep defects.[21,33]

A different approach has been found to account quite well for the observed dependence of the deep defect density across the range of alloy compositions we have studied. A few years ago Stutzmann proposed a "spontaneous bond breaking" model that does not invoke thermal equilibrium arguments.[36] Instead, dangling bonds are thought to be created spontaneously during growth from band tail states lying beyond a certain demarcation energy above the valence band edge; i.e., "weak bonds". Thus, in this model the number of dangling bonds depends solely on the slope of the Urbach tail, E_o, and the demarcation energy, E_{db}. In particular, if the valence bandtail density of states is described by

$$N_{tail}(E) = N^* \exp[-(E^*-E)/E_o] \qquad (10)$$

where $N^* \approx 10^{21}$ cm^{-3} is the band density of states at $E^* = E_v + 0.15$eV, then the number of defects spontaneously created during growth is

$$N_D = \int_{E_{db}}^{\infty} N_{tail}(E)\,dE = E_o N^* \exp[-(E_{db} - E^*)/E_o] \qquad (11)$$

With Eq.(11) Stutzmann was able to fit the dependence of the defect densities on the Urbach energy for a large number of amorphous silicon samples using a single value of the demarcation energy parameter: $E_{db} = 0.55$ eV above E^*, or 0.7eV above E_v. This means the demarcation energy is positioned roughly 0.15eV below the peak position of the dangling bond peak as determined by sub-band-gap optical spectroscopy.

For our silicon-germanium alloys we decided to determine the energy position of E_{db} appropriate to the midgap defect in a similar fashion to find out whether Eq. (11) might also provide a good predictor of the density of defects within the mid-gap defect band of the alloys. That is, we took the defect band positions as plotted in Fig. 16 and subtracted an energy of order the defect half-width (roughly 0.1eV, the value of sigma determined by fitting our photocapacitance/photocurrent spectra assuming Gaussian distributions for the defect bands). Because the defect position vs. germanium content displayed in Fig. 16 obeys the relation

$$E_D - E_V = E_{04}/2 - 50\text{meV} \tag{12}$$

fairly accurately, this implies that, to a first approximation, we can predict the defect densities using the relation

$$N_D \approx 10^{21}\, E_o \exp[-(E_{04}/2 - \Delta E)/E_o] \tag{13}$$

where ΔE includes the difference between E^* and E_V, the sigma of the defect band and the 50meV average offset between E_{04} and the defect position in Eq. (12). That is, ΔE should have a value of roughly 0.3eV.

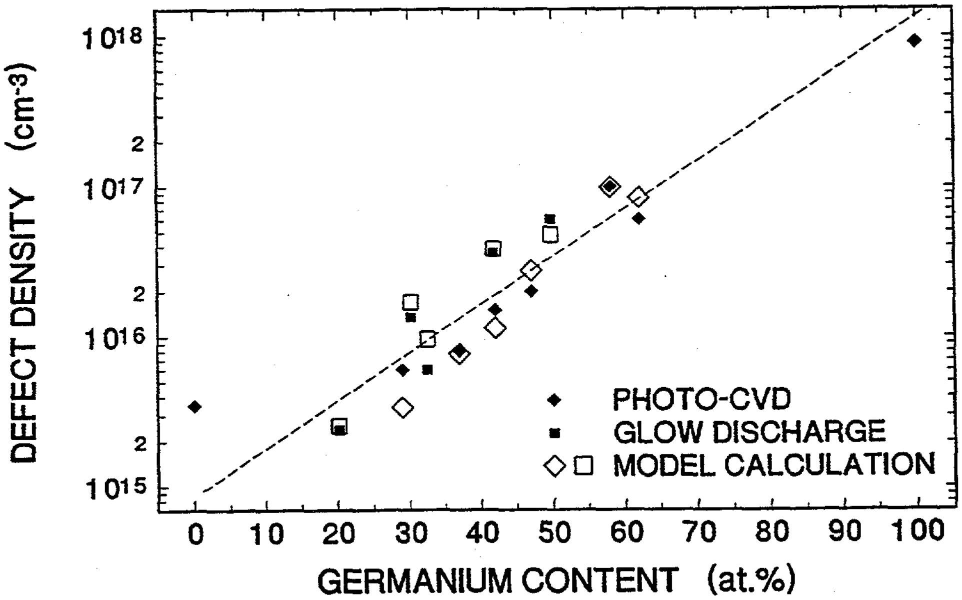

FIG. 17. Deep defect density vs. Ge content for the a-Si,Ge:H alloys: experiment and theory. The solid symbols are the experimental defect densities determined by drive-level profiling, the dashed line is the predicted dependence using the spontaneous bond breaking model assuming a constant Urbach energy of 53meV. The open symbols were calculated using the same model but incorporated the measured Urbach energy for each sample.

Using this value together with the average value of E_0 of 53meV gives a prediction for N_D vs. alloy composition that is plotted as the dashed line in Fig. 17 along with the defect densities determined experimentally by our drive-level capacitance profiling measurements. We see that very good agreement is found with the measured values: the overall dependence is reproduced exactly and the individual values are all reproduced within a factor of two. Better agreement is found if we incorporate the specific values of E_0 determined via the sub-band-gap optical spectra for each sample. These predictions are shown as the open symbols in Fig. 17 and reproduce the measured values to better than a factor of 1.5 in most cases. This agreement with the model applies equally well to the photo-CVD and to the glow discharge samples.

Such a result suggests that the observed increase in the defect density with germanium alloying is really the result of the intrinsic electronic structure of the alloys rather than a lack of optimization of the material. Since the midgap defect band seems to track the middle of the gap [Eq.(12)], this means that once the optical gap and Urbach tail energies are known, the deep defect density is also determined. Thus, further optimization of the a-Si,Ge:H alloys in terms of deep defect density for a given value of optical gap seems to rest completely on the ability to further decrease the width of the valence bandtail. Unfortunately, it is very doubtful that E_0 can be decreased much below 50meV for alloys of compositions relevant to tandem cell development.

5.3 DEFECT RELATED THERMAL TRANSITIONS

In addition to the two optical bands of defect transitions, we have identified two bands of thermal transitions. The first is that found by our drive-level profiling measurement technique which, as we have described in Section 3.2, can also give us information about the *thermal energy distribution* of these defects. This is accomplished by carrying out drive-level profiling measurements at a series of increasing temperatures, plotting the spatially averaged profiles vs. the corresponding thermal emission energies, E_e, as defined by Eq. (3), and then taking the derivative of N_{DL} with respect to E_e to obtain $g(E_e)$ [see Eq. (2)]. This procedure was illustrated in Fig. 2 and 3 for one a-Si,Ge:H sample, and examples for two other samples analyzed in this manner are show in Fig. 18.

Whereas capacitance profiling measurements disclose the depletion charge and hence the distribution of gap states deeper than the bulk Fermi level, the modulated photocurrent (MPC) method is used to investigate the distribution of states that are normally *unoccupied* in the bulk. This technique has been described in Section 3.4. In this case we normally obtain the dependence of the gap state distribution on E_e by scanning the *frequency* of the modulation of the light source for a fixed value of temperature. Repeating this procedure for different fixed temperatures allows us to confirm that these distributions obey thermally activated behavior. We are then able to find the corresponding value of the thermal emission prefactor to convert the frequency scale into a thermal energy scale.

FIG. 18. Drive-level densities and the corresponding densities of states for two a-Si,Ge:H glow discharge samples. The solid symbols are obtained by spatially averging the drive-level profiles for a series of measurements make at increasing temperatures. The open symbols show the underlying densities of states and are obtained by differentiating the drive-level curves with respect to the corresponding thermal emission energies.

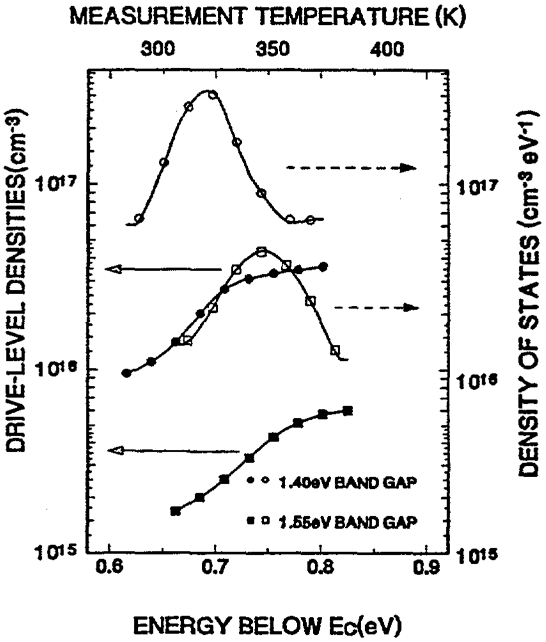

FIG. 19. Density of states obtained by modulated photocurrent measurements by scanning frequency for a series of fixed temperatures. The frequencies for the peak positions at each temperature exhibit thermally activated behavior (inset) which allow us to plot these distributions on a thermal energy scale (see Fig. 20).

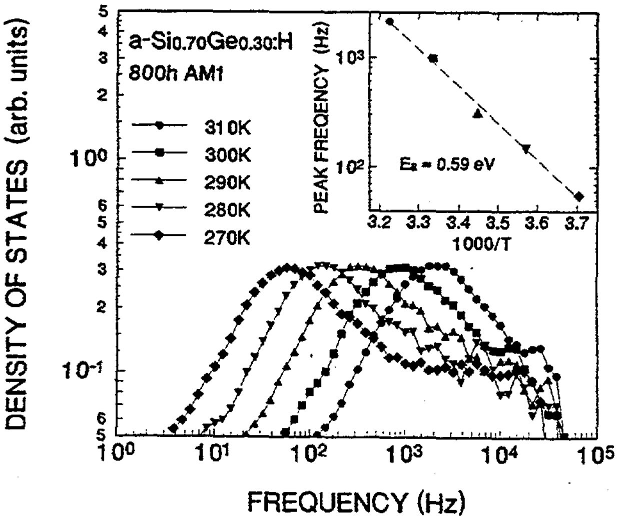

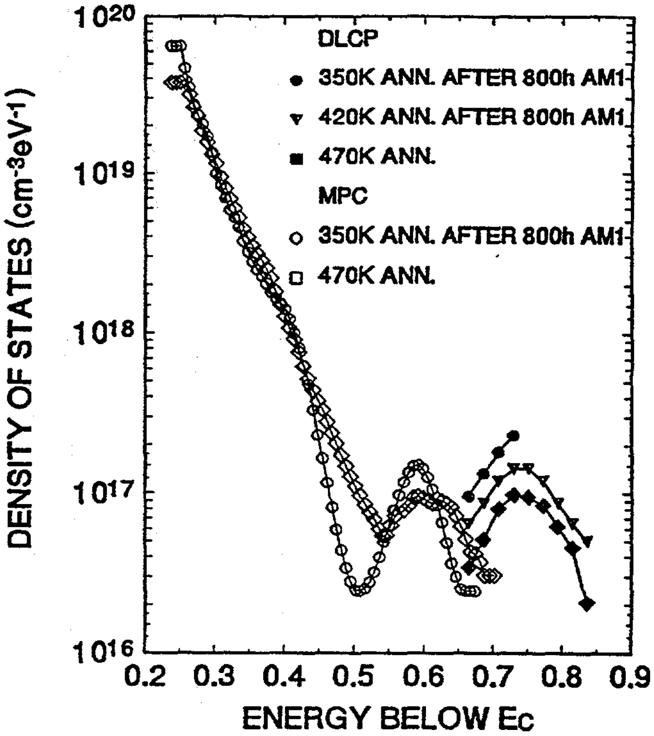

FIG. 20. Defect densities vs. thermal energy derived for the 30at.% Ge glow discharge sample from drive-level profiling and modulated photocurrent measurements. These distributions are shown for the dark annealed state as well as two metastable states following 800 hours of light soaking at AM1 illumination.

An example of an MPC derived gap state distribution is plotted in Fig. 19 *vs.* log(frequency) for several temperatures. In all cases we have scanned the frequency of the light modulation between a few Hz to 100kHz. In Fig. 20 we plot the MPC derived densities of states vs. E_e (for several metastable states of the sample) along with the distributions obtained from the drive-level profiling measurements for the same a-Si,Ge:H sample. The energy scale for both measurements is identical; however, the magnitude of the MPC derived distributions is *not* known as an absolute quantity (in contrast to the drive-level profiling derived distributions). Hence the vertical scale factor chosen to display these data could be uncertain by as much as an order of magnitude.

Using our best estimate of the MPC scale factor, however, indicates that the two thermal bands of defect transitions in the a-Si,Ge:H samples in this generally composition range have nearly equal magnitudes and distributions. Both measurement methods disclose narrow defect sub-bands: a FWHM of roughly 100meV in both cases, located at E_c - 0.75eV for the drive-level derived distributions, and at E_c - 0.59eV for the MPC distributions. As also indicated in Fig. 20, both bands show similar increases in magnitude if the defect density is increased by light soaking.

5.4 IDENTIFICATION OF DEFECT BANDS IN a-Si,Ge:H

We present a schematic representation of the observed optical and thermal transitions in Fig. 21 by summarizing the results that we have obtained. The two optical bands of defect transitions are denoted as OP1 and OP2, while the two thermal bands of defect transitions are denoted as TH1 and TH2. Due to the presence of a single type of defect ESR line in these samples regardless of whether measurements are carried out in the dark or with bias light (or light modulation), we believe that all of the defect transitions correspond to a single type of defect (most likely the Ge dangling bond) that can exist in three charge states: D^+, D^0, and D^-. In this Section we will try to narrow down the identification of the observed transitions as much as possible. However, many of our assignments at this stage must still be regarded as tentative. We are currently carrying out additional ESR measurements which, we believe, will shortly enable us to *unambiguously* identify the four bands of defect transitions we have observed in the a-Si,Ge:H alloys.

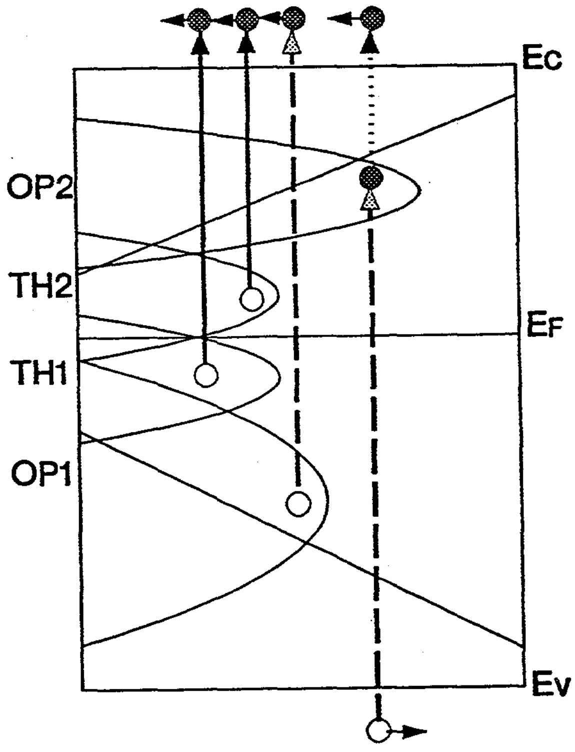

FIG. 21. Schematic showing the two thermal transitions (solid lines) and the two optical transitions (dashed lines) that have been identified in the a-Si,Ge:H alloy samples. The dotted line indicates the suppressed thermal transition as discussed in the text. We have labeled these four defect related transitions as TH1, TH2, OP1, and OP2. For the 30at.% Ge glow-discharge sample these have the approximate energy thresholds of 0.75eV, 0.6eV, 0.85eV, and 1.3eV, respectively.

Because we know that some of the transitions involve adding an electron to the defect while others arise by removing an electron from the defect, the possibilities that could be responsible for the observed bands of transitions are listed as follows:

(1) TH1: D^-/D^o or D^o/D^+ (a defect electron is thermally emitted to the conduction band)

(2) TH2: D^-/D^o or D^o/D^+ (a defect captures a photogenerated electron, then thermally re-emits it to the conduction band)

(3) OP1 D^-/D^o or D^o/D^+ (a defect electron is optically excited into the conduction band)

(4) OP2: D^+/D^o or D^o/D^- (an electron is optically excited into an empty defect state from the valence band)

We are certain that OP2 and TH2 correspond to two *distinct* types of defect sub-bands because the electron added to the defect band by the OP2 transition is not easily thermally emitted to the conduction band, while the electron captured in the TH2 process can re-emitted quite quickly. We also suspect that TH2 is a D^-/D^o transition arising from the D^o sub-band. This is based on the fact that it exhibits an nearly identical thermal emission prefactor compared to that same transition in a-Si:H [37]. This means that OP2 should be identified with a D^+/D^o transition arising from the D^+ sub-band of the defect. Indeed, this is quite consistent with it having a larger thermal barrier to lose its electron to the conduction band. (The thermal emission energy would be larger by at least U_{eff}, the effective correlation energy). This assignment is also supported by the fact that the strength of the OP2 optical transition was significantly larger for one sample that was actually π-type (see Section 5.1).

Fitting the photocapacitance and photocurrent spectra yielded a broad midgap defect band (labeled as OP1) with a FWHM of about 0.2eV. On the other hand, the defect band corresponding TH1 is quite narrow (FWHM~0.1eV). This suggests that the defect bands for OP1 and TH1 may not be the same. This is to be contrasted to a-Si:H where the bands for midgap thermal transitions and optical transitions appear to have nearly identical distributions [13].

If defect relaxation plays a role in the a-Si,Ge:H alloys as it appears to do in a-Si:H [38,39], there could be up to four distinct transitions that would be observed experimentally for given type of defect. We list these using Branz's notation [40]:

(1) $D^-(Q^-)/D^o(Q^-)$: a relaxed D^- state loses an electron to become an unrelaxed D^o state.
(2) $D^o(Q^o)/D^-(Q^o)$: a relaxed D^o state gains an electron to become an unrelaxed D^- state.
(3) $D^o(Q^o)/D^+(Q^o)$: a relaxed D^o state loses an electron to become an unrelaxed D^+ state.
(4) $D^+(Q^+)/D^o(Q^+)$: a relaxed D^+ state gains an electron to become an unrelaxed D^o state.

In this scheme, TH2 would correspond to $D^o(Q^o)/D^-(Q^o)$ since this state starts out as a relaxed D^o state and then captures (and quickly thermally re-emits) an electron. Similarly, OP2 would be assigned to $D^+(Q^+)/D^o(Q^+)$ since it normally exists as a $D^+(Q^+)$ state and then has an electron inserted via an optical transition from the valence band. We suspect OP1 is $D^-(Q^-)/D^o(Q^-)$ since it mimics that optical transition in a-Si:H (a broad midgap band of optical transition).

This leaves two options to assign to TH1. If the defect sub-band slightly above midgap is D^o, then TH1 would correspond to $D^o(Q^o)/D^+(Q^o)$. This assignment is attractive because it would explain why this band has a nearly identical shape to TH2: namely, the $D^o(Q^o)/D^+(Q^o)$ band is the partner of the $D^o(Q^o)/D^-(Q^o)$ band (corresponding to TH2) simply shifted downward in energy by U_{eff} (0.15eV in this case). This assignment would contrast with that of the midgap defect band of thermal transitions in a-Si:H which is generally believed to be associated with the D^-/D^o transition; however, this might be consistent with the lower value of U_{eff} expected for the Ge dangling bond compared to the Si dangling bond.

An alternative would be to identify *both* TH1 and OP1 with the $D^-(Q^-)/D^o(Q^-)$ transition. The apparent difference in their energy distributions would then be attributed to differences that often occur when comparing optical and thermal transitions from deep defects, resulting from relaxation effects associated with that transition. This would increase the optical threshold of the optical transition compared to the thermal transition, and also make it appear somewhat broader.

In principle, a technique such as depletion-width-modulation ESR [41] is the most reliable method to unambiguously identify TH1. While we have not yet been able to carry out such measurements on these alloys due to the special sample requirements, we expect to have such an identification in hand within the next 6 months.

6.0 LIGHT INDUCED DEGRADATION IN a-Si:H AND THE a-Si,Ge:H ALLOYS

6.1 THE EFFECTS OF CARBON IMPURITIES ON LIGHT-INDUCED DEFECT CREATION IN a-Si:H

The effect of impurities upon light-induced metastable defect creation in a-Si:H continues to be controversial. Some early measurements indicated an effect due to impurities in concentrations above 1at.% [42,43], and later evidence for an apparent correlation was found between the level of carbon impurities and the concentrations of light-induced defects.[5] In 1990 our own group demonstrated a strong correlation in samples with varying levels of carbon impurites below the 1at.% level. We carried studies for a-Si:H whose carbon content had been intentionally modulated by varying the gas mixture during growth and then compared the spatial dependence of the SIMS determined carbon concentration profiles with the spatial distributions of light-induced defects obtained using drive-level profiling measurements.[44]

Other researchers, however, have indicated no correlation between low impurity levels and light-induced degradation. The experiments of Shimizu, et. al.[45] show an effect on the dark and photo-conductivity with the addition of 1at.% of nitrogen and oxygen, but show littel effect for the same level of carbon. They also found little effect on the light-induced degradation of such samples. Such types of studies have led to a general acceptance of the idea that light-induced defect creation is predominantly an intrinsic effect in a-Si:H.

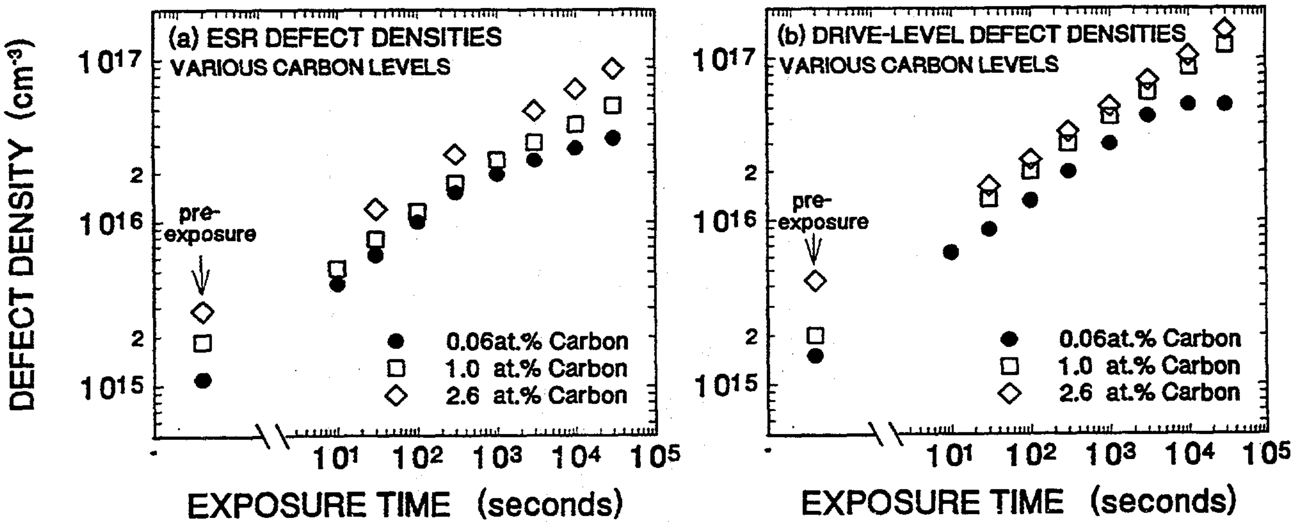

FIG. 22. Comparison of the increase of deep defects with light exposure for 3 a-Si:H samples with varying levels of carbon contamination. This increase in defect density is determined using two experimental methods: electron spin resonance (ESR) and drive-level capacitance profiling (DLCP).

Because of the potential importance of this issue, we have been carrying out additional studies under this Subcontract to examine the matter further. Our results are reported below and, although they do not indicate dramatic effects, they do definitely indicate that carbon impurities at the 1at.% level significantly affect the saturated light-induced defect density in a-Si:H. To reach this conclusion we applied several experimental techniques in tandem. These were electron spin resonance (ESR), the drive-level profiling method, and sub-band-gap spectroscopy (specifically, transient photocurrent spectroscopy). This combination of methods has allowed us to examine changes in different regions of the mobility gap (all of these methods have been described in detail in Section 3). Thus we have been able to document in some detail the changes that occur due to the addition of carbon impurities.

As discussed in Section 3.5, there is a remakable one-to-one correlation between the defect densities established by ESR and the drive-level profiling method over the entire range of light soaked and partially annealed metastable states (see Fig. 6). In Figure 22 we compare the increase of deep defects using both of these methods as a function of light soaking for 3 films with different levels of carbon impurities. Both techniques indicate an increase by factor of 1.5 in the stable defect density when 1at.% of carbon is incorporated and a factor of 2.5 to 3 increase when 2.6at.% is added. This difference of a factor of 3 in defect density is also present between the 2.6at.% contaminated sample and the most intrinsic sample for the most heavily light soaked state of these samples, even though the overall defect densities have been increased by a factor of 30 in all cases. Also, while the most intrinsic sample appears to be showing saturation after 10 hours of our high intensity light soaking (4.5W/cm^2), no such saturation is apparent for the carbon contaminated samples.

In Figure 23(a) the transient photocurrent spectra for state A and state B of the sample containing 2.3% carbon are shown. We observe that the defect absorption increases by roughly a factor of 30 between state A and state B, which is in good agreement with the values found from drive-level profiling and ESR. In figure 23(b) we show a comparison between the transient photocurrent spectra for the most fully light-soaked states of all samples. One notes that the spectra for the different samples have very similar shapes, and, furthermore, that the sample containing 2.6at.% carbon exhibits a factor 2 higher defect absorption than the sample with the lowest carbon content. This is also in good agreement with the drive-level profiling and ESR measurements. All optical spectra are consistent with transient photocapacitance measurements reported earlier [13,14*] that show a dominant defect band located roughly 0.9eV below the conduction band. In Table I we have summarized the electronic properties of the samples determined by our measurements. In addition to the increases in deep defect densities, we observe that the Urbach tail energies increase with alloying with carbon.

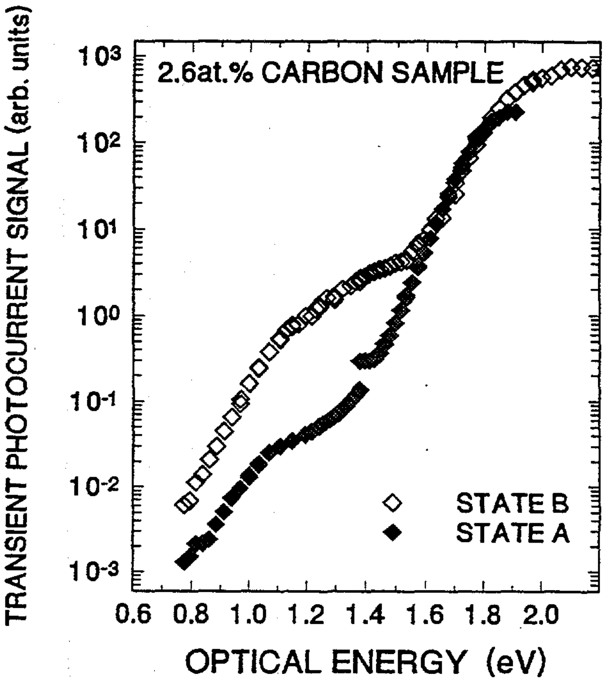

FIG. 23.
(a) Comparison of the transient photocurrent spectra for the a-Si:H sample with 2.6at.% carbon for states A and B. The factor of 30 increase in the defect band agrees with the increase indicated by both the ESR and the DLCP measurements (see Fig. 22).

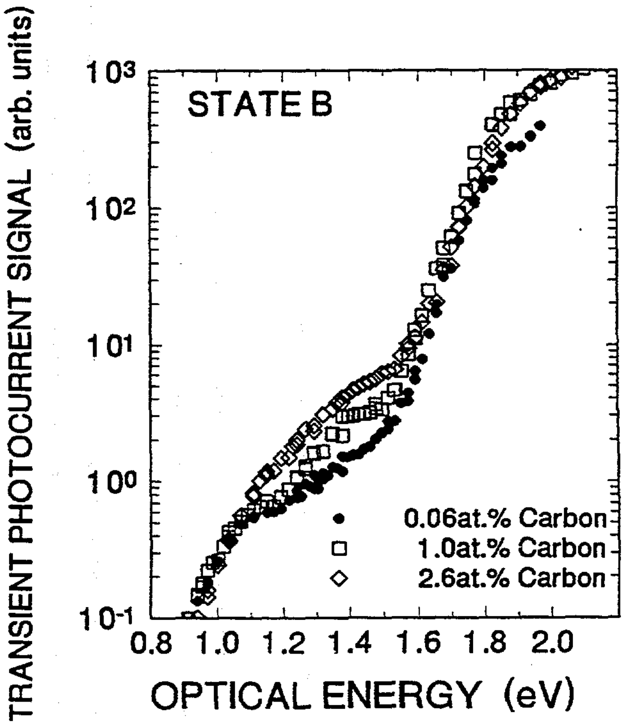

(b) Comparison of the transient photocurrent spectra in state B for three a-Si:H samples with different levels of carbon. The difference between the defect levels between the highest carbon level sample and the most intrinsic sample is roughly a factor of 2. This again agrees with the results of the ESR and DLCP measurements.

TABLE I. Summary of results for light-Induced defect creation for a-Si:H films with varying levels of carbon impurities. Defect densities listed were determined both by ESR (N_s) and drive-level profiling (N_{dl}) and are given both for the dark annealed state (state A) and the metastable state attained after 10 hours of light-soaking at 4.5 W/cm^2 (state B). Band-tail (Urbach) energies determined from sub-band-gap spectroscopy are also indicate.

Sample	[C] (cm^{-3})	E_u (meV)	$N_s(A)$ (cm^{-3})	$N_{dl}(A)$ (cm^{-3})	$N_s(B)$ (cm^{-3})	$N_{dl}(B)$ (cm^{-3})
1	$3\text{x}10^{18}$	52	10^{15}	$1.5\text{x}10^{15}$	$3.4\text{x}10^{16}$	$5.2\text{x}10^{16}$
2	$5\text{x}10^{20}$	55	$1.8\text{x}10^{15}$	$2\text{x}10^{15}$	$5.5\text{x}10^{16}$	$1.2\text{x}10^{17}$
3	$1\text{x}10^{21}$	59	$2.8\text{x}10^{15}$	$4\text{x}10^{15}$	$9\text{x}10^{16}$	$1.5\text{x}10^{17}$

Perhaps the most notable deleterious effect due to carbon impurities as reported above is the lack of saturation of the light-induced effects compared to a-Si:H without carbon. Most recent experiments have found that the defect density under light-soaking does saturate after sufficiently long times. [46,47] However, it is currently being debated whether this saturation is due to an exhaustion of precursor sites or if it is due to a balance of light-induced creation and thermal annealing of defects (or possibly due to both effects). Although it is generally found that the saturation defect density depends on the temperature at which degradation takes place, there is disagreement about the details of this dependence. For example, in the experiments of the Princeton group saturation was achieved after 5 hours with $G = 3\text{x}10^{22}\text{cm}^{-3}$ at a temperature ≤ 90°C. However, in our experiments saturation was not complete after 9 hours at a higher carrier generation rate ($G = 4.5\text{x}10^{22}\text{cm}^{-3}$) and lower temperatures (≤ 70°C). Indeed, the sample with 2.6at.% carbon exhibits an almost perfect $t^{1/3}$ increase in defect density throughout the entire measurement time scale. It is also interesting to note that similar behavior was observed by Shimizu et al., who have found that their carbon contaminated films did not saturate at times when saturation was clearly exhibited for their intrinsic films. [45] In fact, their data indicate that the sample containing carbon began to saturate only after more than 500 hours of illumination at an intensity of $G = 1.6\text{x}10^{22}\text{cm}^{-3}$.

A possible explanation for this behavior is that the incorporation of carbon into a-Si:H increases the activation energy for annealing of metastable defects. This would cause the metastable defect density to saturate at later times and higher values. However, the annealing behavior of our samples does not seem to change significantly for the samples with different levels of carbon. Therefore, we suspect that the increase in metastability is due to an actual *increased susceptibility* to light-induced degradation. This would also lead to saturation at higher values and later light-soaking times.

Since the effect of the carbon impurities is very weak, (roughly one additional metastable defect for 5000 atoms added) we are now inclined to doubt that this increase in susceptibility arises from the direct involvement of carbon atoms in the degradation. Rather, we believe that this increased metastability is caused by an alloying effect, namely, by the increase in the Urbach slopes and in the band gap of the material when carbon is added (see Table I). A similar correlation between the band gap and the light-induced defect density of a-Si:H has also been observed in several other experiments [47,48]. It seems likely that the larger band gap together with the larger number of band-tail states leads to an increased tail-tail recombination energy of free carriers, which allows more potential (band tail) sites to be converted into dangling bonds. Since the band gap increases only slightly for small additions of carbon, only a weak increase in the metastable defect density is expected, in agreement with our experimental results.

6.2 PRELIMINARY STUDIES OF LIGHT-INDUCED DEGRADATION IN THE a-Si,Ge:H ALLOYS

In Figure 24 we display photocapacitance and photocurrent spectra before and after light soaking for a photo-CVD grown alloy sample containing 29at.% Ge. [49] The light exposure in this case consisted of a 50 hour exposure at 400mW/cm^2 from a filtered ELH source. Both pairs of spectra in Fig. 24 were taken in the high temperature regime (350K) so that we could clearly observe the effects of any hole processes. For state A (the lower spectra with the square symbols) we observe a fair amount of splitting in the bandtail regime for the two kinds of spectra indicating a reasonable value of $(\mu\tau)_h$ of about 1.5×10^{-9} cm^2/V. After light soaking (the upper spectra with circle symbols) this splitting is substantially reduced which indicates a dramatic decrease in $(\mu\tau)_h$, to about 4×10^{-10} cm^2/V. In addition, we observe an almost factor of 3 increase in the defect band absorption (the feature near 1.0 eV). This has been made more evident by the dashed curve in Fig. 24(a) which is a re-plot of the state B photocurrent spectrum on top of the state A photocurrent spectrum so that they can be

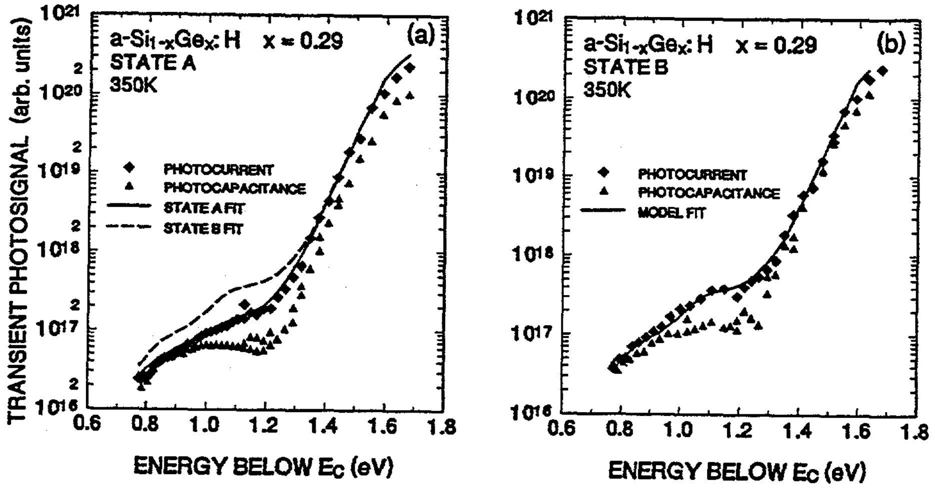

FIG. 24. (a). Transient photocurrent and photocapacitance spectra for the dark annealed state of an $x = 0.29$ a-$Si_{1-x}Ge_x$:H photo-CVD grown sample. The solid lines drawn through the photocurrent data represents the model fit to obtain the defect band transition energies. The dashed line is the state B photocurrent dependence and is drawn to show that the deep defect band has increased by roughly a factor of 3 after light soaking. (b) Transient photocurrent and photocapacitance spectra for the same sample (and same measurement temperature) after light soaking. The solid line is again a model fit. Note that the ratio of the photocurrent/photocapacitance spectra in the tail region has decreased markedly compared to the state A spectra.

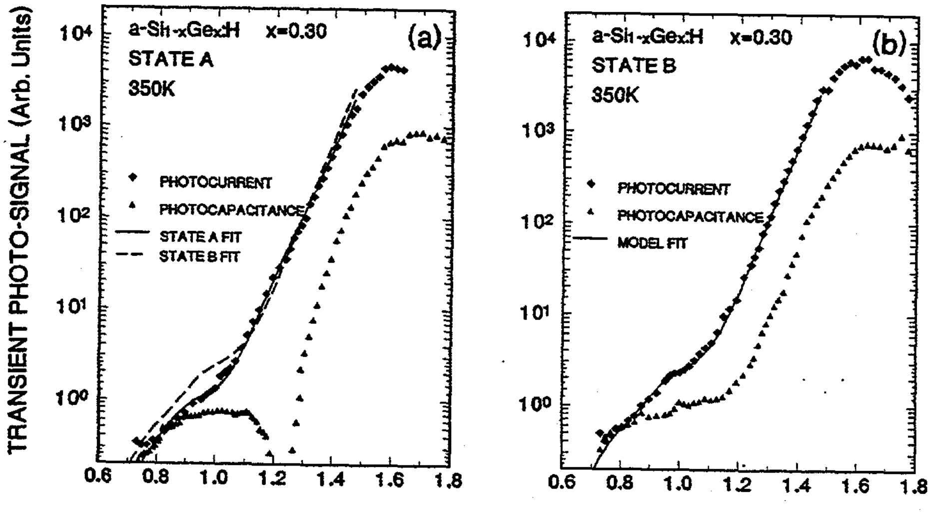

FIG. 25. (a). Transient photocurrent and photocapacitance spectra for the dark annealed state of an $x = 0.30$ a-$Si_{1-x}Ge_x$:H glow-discharge grown sample. Again, the solid lines drawn through the photocurrent data represents the model fit to obtain the defect band transition energies. The dashed line is the state B photocurrent dependence and is drawn to show that the deep defect band has increased by roughly a factor of 2 after light soaking. (b) Transient photocurrent and photocapacitance spectra for the same sample (and same measurement temperature) after light soaking. The solid line is again a model fit. Note that the ratio of the photocurrent/photocapacitance spectra in the tail region is, for this sample, nearly unchanged.

compared directly. A very similar factor increase (2.7) was also obtained by our drive-level evaluation of the deep defect densities.

A similar set of data is presented in Fig. 25 for one of the USSC glow discharge samples with a similar Ge content (30.2at.%). The light exposure in this case was 800h at AM1 and was actually carried out at USSC to allow comparisons with degradation studies in their companion cells. Both pairs of spectra are shown for the same measurement temperature (350K) as for the data in Fig. 25.

We can note both differences and similarities between the two types of samples. First of all, the drive-level profiling data on both the photo-CVD and glow discharge sample exhibit similar increases (roughly a factor of 3) after light soaking (Fig. 20 displays the drive-level derived defect densities for the glow discharge sample). Also, both show a general increase in the defect band portion of the spectra after light soaking (the region below 1.2eV in Figs. 24 and 25). This appears less pronounced in the photocurrent spectra for the glow discharge sample; however, the effect on the photocapacitance spectra appears more dramatic since it completely eliminates the negative signal region for that sample. In addition, the photocurrent spectra for both samples show a distinct shoulder that appears near 1eV following light soaking. This suggests the creation of deep defects in a particular charge state.

On the other hand, the dramatic degradation in the hole $\mu\tau$ product for the photo-CVD sample does not appear to be reproduced for the glow discharge sample; that is, the splitting of the photocapacitance and photocurrent spectra in the bandtail region is nearly unchanged.

Until more of our samples are investigated in this fashion we do not think that definite reasons for the observed types of behavior can be proposed. We suspect that the different behavior for $(\mu\tau)_h$ is probably related to the π-type character of the glow discharge sample. Although a few other photo-CVD samples have been tested and generally show a degradation in $(\mu\tau)_h$ consistent with the increase in the deep defect densities[50], we have not carried out light degradation studies on any of the other glow discharge a-Si,Ge:H films. Since most of those other samples are not π-type to nearly the same degree, it will be particulary interesting to see whether they show the same degradation in $(\mu\tau)_h$ as the photo-CVD samples.

7.0 SUMMARY AND CONCLUSIONS

In this report we have described the results of a fairly complete characterization of a series of a-$Si_{1-x}Ge_x$:H samples grown at the University of Delaware by the photo-CVD method and a series grown at U.S.S.C. by the glow discharge method. We also carried out a more detailed study of the effects of carbon impurities on the light induced degradation in a-Si:H.

Our most general conclusion regarding our work on the low gap alloys is that both series of samples we have studied seem to represent what is close to the "state-of-the-art" in current a-Si,Ge:H alloys. That is, by comparing our results with corresponding values given in the literature, we find equal or superior properties in terms of bandtail widths and stable defect densities. This high quality of the photo-CVD samples is consistent with a statement put forward in an earlier study of glow discharge a-Si,Ge:H; namely, that as the rf power level was decreased, the sample properties were observed to improve monotonically.[10] Although we do not know the details of the deposition parameters for the U.S.S.C. glow discharge films, their use of disilane as the silicon source gas does indeed point toward rather low rf power densities in their growth process. Our detailed comparison of the properties of the glow discharge material with the photo-CVD samples show remarkable similarities rather than significant differences. In particular, our studies do not indicate why the glow discharge material should be superior to the photo-CVD material in cells, although we did find much greater spatial uniformity of electronic properties for the U.S.S.C. grown samples. One U.S.S.C. sample in particular exhibited superior hole transport properties, but we still need to verify that this film is truly reprentative of the material they incorporate into their cells. Also, there may be significant differences in the electronic properties once these samples are degraded; however, results at this stage are still too preliminary to come to any definite conclusions.

The specific scientific conclusions resulting from work under this Subcontract are as follows: First, we can assign defect energy levels from a detailed analysis of our transient sub-band-gap photocapacitance and photocurrent spectra. We find clear evidence for two distinct defect sub-bands, one at roughly midgap and the other in the upper half of the gap, above E_F. We also determined the energy dependence of these defect bands within the gap as the Ge alloy fraction, x, was varied. We found that the midgap defect level appeared to track the conduction band more closely than the valence band (for the shallow level our data was insufficient to decide whether it followed one band more closely). The shallow level was also found to exhibit a suppression of its thermal release of trapped electrons. This suggests a large degree of defect relaxation, as has been discussed previously [5,6].

Second, the density of deep defects is found to increase exponentially with the germanium content. Further, this detailed dependence can be accounted for using a spontaneous bond-breaking model using parameters that can be determined independently from the width of the Urbach tail and the positions and widths of the defect bands found by the analysis of the sub-band-gap optical spectra. This result implies that the alloy samples we have studied may already be quite close to a definite lower limit to the defect densities that can be achieved in this material.

Third, we have found that the trapping lifetime related $\mu\tau$ products for holes decrease in direct proportion to the density of midgap defects in these samples. However, at Ge composition fractions exceeding 50at.% there appears to be an additional decrease in $(\mu\tau)_h$ on top of this. We tentatively attribute this to a larger proportion of charged defects in such samples.

Fourth, we have made significant progress toward identifying both the optical and thermal defect transitions in the a-Si,Ge:H alloys. In addition to the two optical bands of transitions mentioned above, we have identified two thermal bands and have pretty good assignments for three out of these four types of defect transitions.

Finally, we have studied the effects of carbon impurities at the 1at.% level on the light-induded degradation of a-Si:H. Our results show significant effects at this level, particularly in that the carbon contaminated material does not seem to exhibit saturation in degradation compared to the most intrinsic sample. We also found that both the stable and light-induced defect levels increased with carbon levels. However, we attribute most of these effects to a broadening of the valence band-tail and a slight widening of the optical gap.

For future study on the low gap alloys, we will pursue our studies of degradation in both series of samples. We will also add a series of alloy samples optimized for higher Ge content in collaboration with William Paul's group at Harvard. And we hope to obtain a-Si,Ge:H samples grown by a variety of other methods (remote rf discharge, hot-wire, etc.) to determine whether the current baseline of properties established by the present samples really represents any kind of optimum limit.

For future studies of degradation in a-Si:H we also plan to obtain samples grown using less convention methods (hot wire, remote discharge, etc.) and at more extreme growth conditions (high silane dilution in H_2, He, etc.). We are also beginning to try some of our characterization techniques directly on p-i-n cells and hope to better establish clear correlates from our measurements with actual device performance.

8.0 SUBCONTRACT SUPPORTED PUBLICATIONS

Thomas Unold and J. David Cohen, "Density of States and Carrier Dynamics in Amorphous Silicon Germanium Alloys and Amorphous Germanium", J. Non-Cryst. Solids **137&138**, 809 (1991).

J. David Cohen, Thomas Unold, A.V. Gelatos, and C.M. Fortmann, "Deep defect structure and carrier dynamics in amorphous silicon and silicon-germanium alloys determined by transient photocapacitance methods", J. Non-Cryst. Solids 141, 142 (1992).

T. Unold, J.D. Cohen, and C.M. Fortmann, "Effect of Light-Soaking on the Density of States and Carrier Dynamics of a-Si1-xGex:H Alloys", Mat. Res. Soc. Symp. Proc. **258**, 499 (1992).

C.M. Fortmann and J.D. Cohen, "Charge-Defect Thermodynamic Equilibrium and Metastable Defects in a-Si:H", Mat. Res. Soc. Symp. Proc. **258**, 383 (1992)

J. Hautala, T. Unold, and J.D. Cohen, "Effect of C impurities in a-Si:H measured by drive-level capacitance, photocurrent, and electron spin resonance", Mat. Res. Soc. Symp. Proc. 297, **375** (1993).

J. Hautala and J.D. Cohen, "Trapping dynamics and charged defects: Light induced studies in a-Si:H and a-Si1-xGex:H", Mat. Res. Soc. Symp. Proc. 297, **667** (1993).

F. Zhong and J.D. Cohen, "Observation of deep defect relaxation processes in hydrogenated amorphous silicon-germanium alloys", Mat. Res. Soc. Symp. Proc. **297**, 735 (1993).

J. Hautala and J.D. Cohen, "ESR studis on a-Si:H: Evidence for charged defects and safe hole traps", J. Non-Cryst. Solids **164**, 371 (1993)..

T. Unold and J.D. Cohen, "Electronic mobility gap structure and the nature of deep defects in amorphous silicon-germanium alloys", J. Non-Cryst. Solids **164**, 23 (1993).

T. Unold, J.D. Cohen, and C.M Fortmann, "Electronic mobility gap structure and deep defects in amorphous silicon-germanium alloys", Appl. Phys. Lett. **64**, 1714 (1994).

F. Zhong, J.D. Cohen, J. Yang, and S. Guha, "The Electronic Structure of a-Si,Ge:H Alloys", Mat. Res. Symp. Proc., in press.

T. Unold, J. Hautala, and J. David Cohen, "The effect of carbon impurities on the density of states and the stability of hydrogenated amorphous silicon", submitted to the Physical Review.

9.0 REFERENCES

1. D.E. Albright, N. Saxena, C.M. Fortmann, R.E. Rocheleau, T.W.F. Russell, AIChE Journal 36, 1555 (1990).
2. S. Guha, J.S. Payson, S.C. Agarwal, and S.R. Ovshinsky, J. Non-Cryst. Solids **97-98**, 1455 (1988).
3. Lang, D.V., Cohen, J.D., and Harbison, J.P., Phys. Rev. B25, 5285 (1982).
4. C.E. Michelson, A.V. Gelatos, and J.D. Cohen, Appl. Phys. Lett. 47, 412 (1985).
5. K.K. Mahavadi, K. Zellama, J.D. Cohen, and J.P. Harbison, Phys. Rev. B35, 7776 (1987).
6. H. Oheda, J. Appl. Phys. **52**, 6693 (1981).
7. G. Schumm and G.H. Bauer, Phys. Rev. B**39**, 5311 (1989).
8. R. Bruggemann, C. Main, J. Berkin, and S. Regnolds, Philos. Mag. B**64**, 515 (1991).
9. K. Hattori, Y. Niwano, H. Okamoto, and Y. Hamakawa, J. Non-Cryst. Solids **137&138**, 363 (1990).
10. Lang, D.V. in Thermally Stimulated Relaxation in Solids, vol. 37 of Topics in Applied Physics, ed by P. Braunlich (Springer, Berlin, 1979), p. 93.
11. Cohen, J.D., in Hydrogenated Amorphous Silicon, vol. 21C of Semiconductors and Semimetals, ed. by J. Pankove (Academic Press, New York, 1984), p. 9.
12. Gelatos, A.V., Cohen, J.D., and Harbison, J.P., in Optical Effects in Amorphous Silicon, ed. by P.C. Taylor and S.G. Bishop (AIP Conf. Proc. No. 120, New York, 1984), p. 16.
13. Gelatos, A.V., Cohen, J.D., and Harbison, J.P., Appl. Phys. Lett., 49, 722 (1986).
14. Cohen, J.D., and Gelatos, A.V., in Amorphous Silicon and Related Materials, ed. by H. Fritzsche (World Scientific, Singapore, 1989), p. 475.
15. Amer, N.M., and Jackson, W.B., in Hydrogenated Amorphous Silicon, vol. 21B of Semiconductors and Semimetals, ed. by J. Pankove (Academic Press, New York, 1984), p. 83.
16. Vanacek, M., Kocka, J., Stuchlik, J., Kozisek, Z., Stika, O., and Triska, A., Sol. Energy Mat. 8, 411 (1983).
17. J. Hautala and J.D. Cohen, Mat. Res. Soc. Symp. Proc. **297**, 375 (1993).
18. T. Unold, J.D. Cohen, and C.M. Fortmann, Appl. Phys. Lett. **64**, 1714 (1994).
19. F. Zhong and J.D. Cohen, unpublished.

20. T Unold, Ph.D. Thesis 1993 (unpublished).

21. S. Aljishi, Z E. Smith, and S. Wagner, in *Advances in Disordered Semiconductors Vol I: Amorphous Silicon and Related Materials*, ed. by H. Fritzsche (World Scientific, Singapore, 1988), pp. 887-938.

22. M. Stutzmann, R.A. Street, C.C. Tsai, J.B. Boyce, and S.E. Ready, J. Appl. Phys. 66, 569 (1989).

23. T. Unold and J.D. Cohen, J. Non-Cryst. Solids **137&138**, 809 (1991).

24. See, for example, J.D. Cohen and D.V. Lang, Phys. Rev. B**25**, 5321 (1981).

25. J.D. Cohen, T. Unold, A.V. Gelatos, and C.M. Fortmann, J. Non-Cryst. Solids **141**, 142 (1991).

26. Note: This expression is in a slightly corrected form from what had appeared in Refs. 4, 5, and 6.

27. F. Zhong, J.D. Cohen, J. Yang, and S. Guha, Mat. Res. Soc. Symp. Proc., in press.

28. L. Chen, J. Tauc, J.-K. Lee, and E.A. Schiff, Phys. Rev. B43, 11694 (1991).

29. Fortmann, C.M., Albright, D.E, Campbell, I.H., and Fauchet, P.M., Mat. Res. Soc. Symp. Proc. 164, 315 (1990).

30. B. von Roedern, Appl. Phys. Lett.62, 1368 (1993).

31. S. Guha, private communication.

32. H. Matsurra, J. Appl. Phys. **64**, 1964 (1988).

33. D. Sella Sala, C. Reita, G. Conte, F. Galluzzi, and G. Grillo, J. Appl. Phys. **67**, 814 (1990).

34. S.S. Hegedus and E.A. Fagan, J. Appl. Phys. **71**, 5941 (1992).

35. W. Paul, J. Non-Cryst. Solids **137&138**, 803 (1991).

36. M. Stutzmann, Philos. Mag. B**60**, 531 (1989).

37. F. Zhong and J.D. Cohen, Mat. Res. Soc. Symp. Proc. **258**, 813 (1992).

38. J.D. Cohen, T.M. Leen, and R.J. Rasmussen, Phys. Rev. Lett. **69**, 3358 (1992).

39. F. Zhong and J.D. Cohen, Phys. Rev. Lett. **71**, 597 (1993).

40. H.M. Branz and E.A. Schiff, Phys. Rev. B**48**, 8667 (1993).

41. J.D. Cohen, J.P. Harbison, and K.W. Wecht, Phys. Rev. Lett. **48**, 109 (1982).

42. D.E. Carlson, A. Catalano, R.V. D'Aiello, C.R. Dickson, and R.S. Oswald, in *Optical Effects in Armophous Semiconductors*, ed. by P.C. Taylor and S.G. Bishop (AIP Conf. Proc. No. 120, New York, 1984), p. 234.

43. R.S. Crandall, D.E. Carlson, A. Catalano, and H.A. Weakliem, Appl. Phys. Lett. **44**, 200 (1984).

44. T. Unold and J.D. Cohen, Appl. Phys. Lett. **58**, 723 (1990).

45. T. Shimizu, M. Matsumoto, M. Yoshita, M. Iwami, A. Morimoto, and M. Dumeda, J. Non-Cryst. Solids **137&138**, 391 (1991).

46. M. Stutzmann, W.B. Jackson, and C.C. Tsai, Phys. Rev. B**32**, 23 (1985).

47. M. Isomura, X. Xu, and S. Wagner, Solar Cells **30**, 177 (1991).

48. A. Skumanich and N.M. Amer, Phys. Rev. B**37**, 8465 (1988).

49. T. Unold, J.D. Cohen, and C.M. Fortmann, Mat. Res. Symp. Proc. 258, 499 (1992).

50. See last year's annual report: J.D. Cohen, Report No. NREL/TP-451-5737 (1993).

REPORT DOCUMENTATION PAGE

Form Approved
OMB NO. 0704-0188

1. AGENCY USE ONLY (Leave blank)

2. REPORT DATE
September 1994

3. REPORT TYPE AND DATES COVERED
Final Subcontract Report, 1 February 1991 - 31 January 1994

4. TITLE AND SUBTITLE
Microscopic Origins of Metastable Effects in a-Si:H and Deep Defect Characterization in a-Si,Ge:H Alloys

5. FUNDING NUMBERS
C: XG-1-10063-1
TA: PV431101

6. AUTHOR(S)
J. D. Cohen

7. PERFORMING ORGANIZATION NAME(S) AND ADDRESS(ES)
University of Oregon
Department of Physics and Materials Science Institute
Eugene, Oregon

8. PERFORMING ORGANIZATION REPORT NUMBER

9. SPONSORING/MONITORING AGENCY NAME(S) AND ADDRESS(ES)
National Renewable Energy Laboratory
1617 Cole Blvd.
Golden, CO 80401-3393

10. SPONSORING/MONITORING AGENCY REPORT NUMBER
TP-451-7163
DE94011887

11. SUPPLEMENTARY NOTES
NREL Technical Monitor: B. von Roedern

12a. DISTRIBUTION/AVAILABILITY STATEMENT

12b. DISTRIBUTION CODE
UC-1262

13. ABSTRACT *(Maximum 200 words)*

This report describes work to characterize two series of a-Si$_{1-x}$Ge$_x$:H samples: a series of nine films grown at the University of Delaware by the photo-chemical vapor deposition (CVD) method (for $0.29 \le x \le 0.62$), and a series of six films grown at United Solar Systems Corporation by the glow discharge method (for $0.20 \le x \le 0.50$). Both series of samples seem to represent what is close to the "state of the art" in current a-Si,Ge:H alloys. Our detailed comparison of the properties of the glow discharge material with the photo-CVD samples shows remarkable similarities rather than significant differences. In addition to our studies of the low-gap materials, we also studied the effects of carbon impurities at the 1 at% level on the light-induced degradation of a-Si:H. Results showed significant effects at this level—particularly, in the carbon-contaminated material, the light-induced defect density does not seem to exhibit saturation in comparison to many other intrinsic samples. We also found that both the stable and light-induced defect levels increased with carbon at these contamination levels.

14. SUBJECT TERMS
hydrogenated amorphous silicon ; defect characterization ; hydrogenated amorphous silicon germanium ; metastability ; photovoltaics ; solar cells

15. NUMBER OF PAGES
53

16. PRICE CODE

17. SECURITY CLASSIFICATION OF REPORT
Unclassified

18. SECURITY CLASSIFICATION OF THIS PAGE
Unclassified

19. SECURITY CLASSIFICATION OF ABSTRACT
Unclassified

20. LIMITATION OF ABSTRACT
UL

NSN 7540-01-280-5500

Standard Form 298 (Rev. 2-89)
Prescribed by ANSI Std. Z39-18
298-102